

Impacts of Degradation on Water, Energy, and Carbon Cycling of the Amazon Tropical Forests

Marcos Longo¹, Sassan Saatchi^{2,3}, Michael Keller^{2,4,5}, Kevin Bowman², António Ferraz^{2,3}, Paul R. Moorcroft⁶, Douglas C Morton⁷, Damien Bonal⁸, Paulo Brando^{9,10,11}, Benoît Burban¹², Géraldine Derroire¹³, Maiza N dos-Santos⁵, Victoria Meyer², Scott Saleska¹⁴, Susan Trumbore¹⁵, Grégoire Vincent¹⁶

¹NASA Postdoctoral Program Fellow, Jet Propulsion Laboratory, California Institute of Technology,
Pasadena CA, United States

²Jet Propulsion Laboratory, California Institute of Technology, Pasadena, CA, United States

³Institute of Environment and Sustainability, University of California, Los Angeles, CA, United States

⁴International Institute of Tropical Forestry, USDA Forest Service, Rio Piedras, Puerto Rico

⁵Embrapa Informática Agropecuária, Campinas, SP, Brazil

⁶Department of Organismic and Evolutionary Biology, Harvard University, Cambridge, MA, United States

⁷NASA Goddard Space Flight Center, Greenbelt, MD, United States

⁸Université de Lorraine, INRAE, AgroParisTech, UMR Silva, F-54000 Nancy, France

⁹Department of Earth System Science, University of California, Irvine, CA, United States

¹⁰Woods Hole Research Center, Woods Hole, MA, United States

¹¹Instituto de Pesquisa Ambiental da Amazônia, Brasília, DF, Brazil

¹²Institut National de Recherche en Agriculture, Alimentation et Environnement (INRAE), UMR 0745

EcoFoG, Campus Agronomique, Kourou 97379, France

¹³Centre de Coopération Internationale en Recherche Agronomique pour le Développement (CIRAD),

UMR EcoFoG (Agroparistech, CNRS, INRAE, Université des Antilles, Université de Guyane), Campus

Agronomique, Kourou 97379, France

¹⁴University of Arizona, Tucson, AZ, United States

¹⁵Max-Planck-Institut für Biochemie, Jena, Germany

¹⁶AMAP, Univ Montpellier, IRD, CIRAD, CNRS, INRAE, Montpellier, 34000 France

Key Points:

- Airborne lidar can be used to inform degradation-driven changes in structure to vegetation models

- 31 • Forest degradation typically depletes evapotranspiration and productivity and in-
32 creases flammability
- 33 • Extreme droughts reduce functional differences between degraded and intact trop-
34 ical forests

Abstract

Selective logging, fragmentation, and understory fires directly degrade forest structure and composition. However, studies addressing the effects of forest degradation on carbon, water, and energy cycles are scarce. Here, we integrate field observations and high-resolution remote sensing from airborne lidar to provide realistic initial conditions to the Ecosystem Demography Model (ED-2.2) and investigate how disturbances from forest degradation affect gross primary production (GPP), evapotranspiration (ET), and sensible heat flux (H). We used forest structural information retrieved from airborne lidar samples (13,500 ha) and calibrated with 817 inventory plots (0.25 ha) across precipitation and degradation gradients in the Eastern Amazon as initial conditions to ED-2.2 model. Our results show that the magnitude and seasonality of fluxes were modulated by changes in forest structure caused by degradation. During the dry season and under typical conditions, severely degraded forests (biomass loss $\geq 66\%$) experienced water-stress with declines in ET (up to 34%) and GPP (up to 35%), and increases of H (up to 43%) and daily mean ground temperatures (up to 6.5°C) relative to intact forests. In contrast, the relative impact of forest degradation on energy, water, and carbon cycles markedly diminishes under extreme, multi-year droughts, as a consequence of severe stress experienced by intact forests. Our results highlight that the water and energy cycles in the Amazon are not only driven by climate and deforestation, but also the past disturbance and changes of forest structure from degradation, suggesting a much broader influence of human land use activities on the tropical ecosystems.

Plain Language Summary

In the Amazon, timber extraction and forest fires ignited by people are the chief causes of damages that we call forest degradation. Degradation is as widespread as deforestation, and changes how forests behave. Degraded forests may pump less water to the atmosphere and absorb less carbon dioxide from the atmosphere. To understand the differences in behavior between degraded and intact forests, we used high-resolution scanning laser data collected from aircraft flights over regions in the Amazon where we knew if and when forests were degraded. Then, we provided these data to a computer program that calculates the exchange of water and carbon between the forest and the atmosphere. We found that, during the dry season, degraded forests are 6.5°C warmer, pump 1/3 less water (i.e., 40,000 L ha⁻¹ month⁻¹), absorb 1/3 less carbon (i.e., 1 tonC ha⁻¹ month⁻¹),

67 and show higher fire risk than intact forests. To our surprise, when the Amazon is hit
68 by severe droughts, intact forests start to behave like degraded forests, because all forests
69 run out of water and become hot. Our results are important because they show that for-
70 est degradation caused by people can have large impacts on dry-season climate and fa-
71 vor more fire, especially during typical, non-drought years.

72 **1 Introduction**

73 Tropical forests account for 25–40% of total carbon stocks in terrestrial ecosystems
74 (Sabine et al., 2004; Meister et al., 2012), but their maintenance and functioning have
75 been weakened by climate and land-use change. As a result, tropical forests may shift
76 to net sources of carbon to the atmosphere, with residence time of carbon in forests de-
77 clining by 50% (Davidson et al., 2012; Grace et al., 2014; Lewis et al., 2015; Erb et al.,
78 2016). Land use and land cover changes contribute to nearly 15% of total annual car-
79 bon emissions (Harris et al., 2012; Friedlingstein et al., 2019). However, most studies as-
80 sessing the effects of land use change on tropical forest stocks and fluxes have focused
81 on the effects of deforestation (e.g., Harris et al., 2012; Achard et al., 2014). Logging,
82 understory fires and forest fragmentation — collectively known as *forest degradation* (Hosonuma
83 et al., 2012) — could play a comparable role in the forest’s energy, water, and carbon
84 cycle and induce locally warmer and drier conditions that could be detrimental to their
85 functioning (Grossiord et al., 2020; Sullivan et al., 2020), but these effects remain poorly
86 quantified.

87 Significant fractions of the remaining tropical forests are located within 1 km from
88 the forest’s edge (Haddad et al., 2015; Lewis et al., 2015) and thus are probably degraded
89 (Asner et al., 2006; Morton et al., 2013; Pütz et al., 2014; Tyukavina et al., 2016; Potapov
90 et al., 2017). The area impacted by forest degradation in the Amazon each year is highly
91 uncertain, but likely comparable to deforestation (Asner et al., 2006; Morton et al., 2013;
92 Tyukavina et al., 2017). Total carbon losses attributable to degradation may be simi-
93 lar or exceed deforestation-related losses in tropical forests (Berenguer et al., 2014; Pear-
94 son et al., 2017; Baccini et al., 2017; Aragão et al., 2018; Erb et al., 2018), and degra-
95 dation may even dominate the carbon losses in indigenous lands and protected areas (Walker
96 et al., 2020). At the local scale, carbon stocks in degraded forests are extremely variable.
97 Lightly disturbed forests (e.g., reduced-impact logging) store as much carbon as intact
98 forests, while forests impacted by severe or multiple disturbances may lose a significant

99 fraction or nearly all of their original carbon stocks (Berenguer et al., 2014; Alamgir et
100 al., 2016; Longo et al., 2016; Rappaport et al., 2018; Ferraz et al., 2018). Transitions be-
101 tween lightly and heavily degraded forests may be non-linear and abrupt (Brando et al.,
102 2014). Unquestionably, estimates of fluxes from forest degradation and regeneration are
103 more uncertain than emissions from deforestation (Aragão et al., 2014; Morton, 2016;
104 Bustamante et al., 2016), because their impacts on forests are more subtle than defor-
105estation and thus more difficult to detect and quantify with traditional remote sensing
106 techniques.

107 Selective logging and fires also modify the forest structure, composition and func-
108 tioning. For example, selective logging in the tropics generally targets large trees (diam-
109 eter at breast height, $DBH \geq 40\text{--}60$ cm) from a few marketable species (e.g., Feldpausch
110 et al., 2005; Blanc et al., 2009; Pinagé et al., 2019), but the other logging structures such
111 as skid trails and log decks kill or damage mostly small trees ($DBH < 20$ cm) (Feldpausch
112 et al., 2005). Likewise, fire mortality decreases with tree size and the bark thickness (e.g.,
113 Brando et al., 2012; Pellegrini et al., 2016), although areas disturbed by recurrent fires
114 also show significant losses of large trees (Barlow et al., 2003; Martins et al., 2012; Brando,
115 Silvério, et al., 2019; Silvério et al., 2019). Consequently, degradation creates more open
116 canopies and thinner understory (e.g., d’Oliveira et al., 2012; Pinagé et al., 2019; Silvério
117 et al., 2019) and increased abundance of grasses and fast-growing, low wood-density tree
118 species (Barlow et al., 2016; Both et al., 2019; Brando, Silvério, et al., 2019).

119 Previous studies indicate an increase in dry-season length in parts of the Amazon
120 where both deforestation and forest degradation are pervasive (e.g., Fu et al., 2013; Sena
121 et al., 2018), and that the onset of the wet season is modulated by forest transpiration
122 (J. S. Wright et al., 2017). Temperature and vapor pressure deficit (VPD), important
123 drivers of evapotranspiration (ET), were found by Kapos (1989) to be significantly higher
124 near forest edges. Likewise, Jucker et al. (2018) installed a network of micrometeorolog-
125 ical measurements across a study area in Sabah, Malaysia, that included intact forests,
126 a broad range of degraded forests and oil-palm plantations, and found that forest struc-
127 ture, along with topographic features, explained most of the variance in understory tem-
128 perature. Yet, only a few studies on experimental sites quantified the magnitude, sea-
129 sonality, and interannual variability of water, and energy cycles in degraded forests. For
130 example, S. D. Miller et al. (2011) analyzed the impact of reduced-impact, low-intensity
131 selective logging in the Amazon using eddy covariance towers and found only minor im-

132 pacts of logging on sensible and latent heat fluxes. Recently, Brando, Silvério, et al. (2019)
133 compared eddy covariance data from two towers at an experimental fire site in the Ama-
134 zon forest, and found declining differences in gross primary productivity and small dif-
135 ferences in evapotranspiration between the control and burned area between 4 and 8 years
136 after the last burn.

137 Field inventory plots are fundamental to sample the structure and species compo-
138 sition of tropical forests, but they also have important limitations to characterize the het-
139 erogeneity of degraded landscapes. First, the number of plots required to characterize
140 stands increase with heterogeneity, often reaching impractical numbers (Marvin et al.,
141 2014). In addition, most tropical forest degradation occurs in private landholdings and
142 privately managed logging concessions, where limited access by researchers may create
143 sampling bias towards well-managed areas, which generally experience less intensive degra-
144 dation. However, airborne laser scanning (airborne lidar) can circumvent these limita-
145 tions over large areas with sub-meter resolution. Airborne lidar data have been used suc-
146 cessfully to quantify structural characteristics of the canopy such as height and leaf area
147 distribution (Hunter et al., 2013; Vincent et al., 2017; Shao et al., 2019). Moreover, these
148 data have also been used to quantify changes in canopy structure and carbon stocks at
149 local to regional scale that experienced multiple levels of degradation (e.g., Asner et al.,
150 2010; Longo et al., 2016; Ferraz et al., 2018; Meyer et al., 2019).

151 Numerical models can be used to understand the links between changes in forest
152 structure, light and water availability for different local plant communities, and the over-
153 all impact on energy, water, and carbon fluxes between forests and the atmosphere. In
154 the past, *big-leaf* models have been modified to account for the long-term impacts of se-
155 lectively logged tropical forests on the carbon cycle of tropical forests (e.g., Huang et al.,
156 2008; Huang & Asner, 2010). However, big-leaf models generally do not represent the
157 mechanisms that control access and availability of light and water in complex and het-
158 erogeneous forest structures (D. Purves & Pacala, 2008; Fisher et al., 2018) (but see Braghieri
159 et al., 2019). Individual-based models can represent the changes in the population struc-
160 ture and micro-environments due to degradation (R. Fischer et al., 2016; Maréchaux &
161 Chave, 2017), but the complexity and computational burden of these simulations often
162 limit their application to single sites. Cohort-based models, such as the Ecosystem De-
163 mography (ED-2.2) model (Medvigy et al., 2009; Longo, Knox, Medvigy, et al., 2019),
164 strike a balance between these end-members because they can efficiently represent the

165 horizontal and vertical heterogeneity of forests. However, to represent the impact of het-
166 terogeneity in the energy, water, and carbon cycles, it is critical that these models are in-
167 formed with realistic initial conditions that capture the landscape variability and they
168 accurately represent the complex interactions between climate and the micro-environment
169 variability. Previous studies using a variety of cohort-based models have demonstrated
170 that cohort-based models can realistically reproduce the micro-environment heterogene-
171 ity and the long-term dynamics of ecosystems, compared to both individual-based mod-
172 els (Moorcroft et al., 2001; Strigul et al., 2008) and observations (D. W. Purves et al.,
173 2008; Longo, Knox, Levine, et al., 2019; Koven et al., 2019).

174 In this study, we use airborne lidar data to quantify forest structure variability across
175 the Amazon in order to provide critical initial conditions for ecosystem demography mod-
176 els. We also investigate the role of forest degradation on the Amazon forest productiv-
177 ity, flammability, as well as the degradation impacts on the water and energy cycles. Specif-
178 ically, we seek to answer the following questions:

- 179 1. What are the relationships between degradation metrics (e.g. biomass loss) and
180 changes in carbon, water, and energy fluxes, and how does it vary across seasons
181 and regions with different rainfall regimes?
- 182 2. How do droughts affect the relationships between degradation and ecosystem func-
183 tioning?
- 184 3. Does forest degradation make Amazon forests more susceptible to fires? If so, which
185 parts of the Amazon experience the largest flammability response to degradation?

186 To this end, we integrate field inventory plots with high-resolution airborne lidar data
187 over five study regions in the Eastern Amazon along a precipitation gradient and with
188 a broad range of anthropogenic disturbance histories, to provide initial conditions to ED-
189 2.2 that realistically represent the structural diversity of degraded forests. While lim-
190 ited to specific regions in the Amazon where detailed degradation information exists, our
191 goal is to provide a framework that can be extended to larger scales, including biome-
192 and pantropical scales.

2 Materials and Methods

2.1 Study regions

We selected five study regions across a gradient of disturbance and climate conditions where ground and airborne lidar are available to study the forest function (Figure 1; Table 1). Three of these sites include eddy covariance tower measurement of energy, water, and carbon dioxide fluxes for comparison with the model simulations, and have been the focus of several ecological studies in the past. Additional details on the disturbance history of each region are available at Text S1.

1. *Paracou, French Guiana (GYF)* is a field station where a logging experiment was conducted between 1987 and 1988 that includes intact forest controls and three selective logging treatments: timber extraction using conventional logging techniques, timber extraction and canopy thinning, and timber and fuelwood extraction followed by canopy thinning (Gourlet-Fleury et al., 2004). The eddy covariance tower at the site is located in the undisturbed forest and has been operational since 2004 (Guyaflux; Bonal et al., 2008).
2. *Belterra, Brazil (BTE)*. Over the past 100 years, this region experienced cycles of economic growth and recession that created a complex landscapes dominated by deforestation, degradation and second-growth. The Tapajós National Forest is this region, and has areas of intact forests and selectively logged forests using reduced-impact techniques (VanWey et al., 2007; Pyle et al., 2008; Lei et al., 2018). An eddy covariance tower known as Km 67 overlaps with one of the surveyed sites and has data for 2001–2005, and 2008–2011 (Hayek et al., 2018).
3. The *Paragominas, Brazil (PRG)* region used to be within the largest timber production area in Brazil and has undergone selective logging since the 1970s (Veríssimo et al., 1992). Since the 1990s, the economy has shifted towards agriculture, introducing large-scale deforestation such that nearly half of the original forest cover has been lost, and most of the remaining areas have been logged (Pinto et al., 2009).
4. *Feliz Natal, Brazil (FZN)* is located at the southern fringe of the Amazon in a mosaic landscape of soybean fields, grazing lands, and logged forests. This region regularly experiences severe dry seasons and frequent understory fires (Morton et al., 2013; Rappaport et al., 2018).

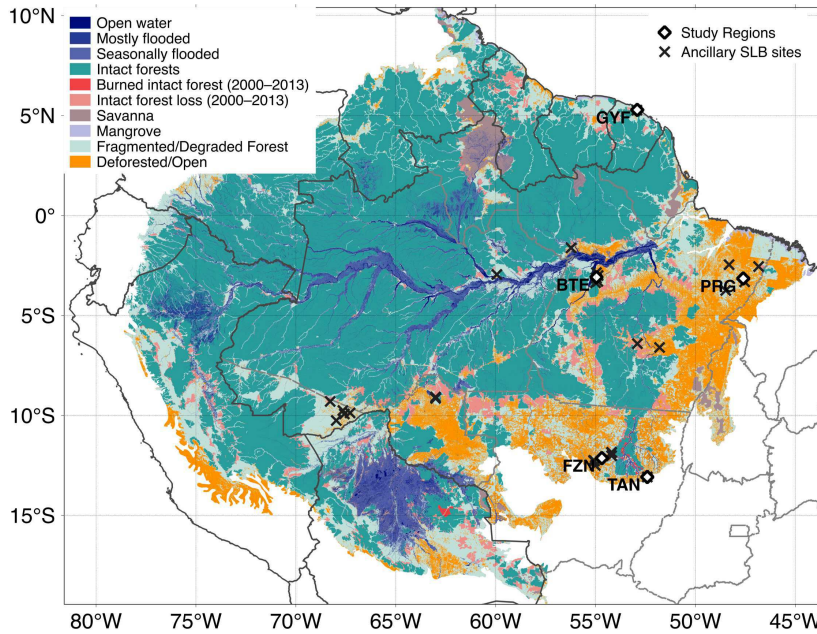


Figure 1. Location of the five study regions within the Amazon biome region, along with land classification as of 2013. Intact forest and intact forest loss were obtained from Potapov et al. (2017); open and deforested areas were obtained from PRODES-INPE (2018) (Brazil) and areas with tree cover below 20% according to Hansen et al. (2013) (other countries); wetlands and water bodies in the Amazon River Basin were from Hess et al. (2015) and savannas and mangroves were obtained from Olson et al. (2001).

224 5. *Tanguro, Brazil (TAN)* is located in an experimental fire study area within a larger
 225 landscape covered by intact forests and forests that were disturbed with low-intensity
 226 understory fires (one, three, and six times) between 2004 and 2010 (Balch et al.,
 227 2008; Brando et al., 2014). The surveyed region also includes two eddy covariance
 228 towers that have been operating since 2014 both at the intact and burned forests
 229 (Brando, Silvério, et al., 2019).

230 These five study regions were sampled at multiple sites by small-footprint, multiple-
 231 return airborne lidar. The lidar data provided both the terrain elevation at high spatial
 232 resolution (1-m) and detailed information about the vertical structure of forests from a
 233 uniform point cloud density to meet a minimum return density of 4 returns per m^2 over
 234 99.5% of the area (Leitold et al., 2015). Living trees of diameter at breast height $\text{DBH} \geq$
 235 10 cm were either botanically identified (experimental plots in GYF) or identified from
 236 field characteristics by local parataxonomists. To characterize the disturbance history,

Table 1. Overview of the study regions, including mean annual precipitation (MAP) and dry-season length (DSL).

Region (Code)	Coordinates	MAP ^a [mm]	DSL ^b [mo]	Lidar [ha]	Inventory [ha]	Disturbances ^c
Paracou (GYF)	5.28°N; 52.91°W	3040	2(0)	963	79.8	INT, CL1, LTH
Belterra (BTE)	3.09°S; 54.95°W	1890	5(1)	4057	16.7	INT, RIL, BN1, BN2, BN3
Paragominas (PRG)	3.15°S; 47.61°W	1850	6(2)	3217	35.6	INT, RIL, CL1, BN1, LB1, BN2, BN3
Feliz Natal (FZN)	12.14°S; 54.68°W	1940	5(4)	4210	14.0	INT, CL1, CL2, BN1, LB1, BN2, BN3
Tanguro (TAN)	13.08°S; 52.41°W	1800	5(4)	1006	22.9	INT, BN1, BN3, BN6

^a Source for mean annual precipitation (MAP) data: GYF – Gourlet-Fleury et al. (2004); other regions – nearest site available at INMET (2019).

^b Dry-season length (DSL): number of months with precipitation below 100 mm; numbers in parentheses indicate number of severely dry months (precipitation below 30 mm).

^c Disturbance history classes: INT – intact; RIL – reduced-impact logging; CL x – conventional logging (x times); LTH – conventional logging and thinning; LB1 – conventional logging and burned (once); BN x – burned x times.

237 we used either published information from the experimental regions GYF (Gourlet-Fleury
 238 et al., 2004; Bonal et al., 2008; Wagner et al., 2013) and TAN (Brando et al., 2012, 2014),
 239 or the disturbance history analysis from (Longo et al., 2016), which was based on a vi-
 240 sual interpretation of the Normalized Burn Ratio (NBR) of cloud-free Landsat images
 241 since 1984, and complemented with information from logging companies for the reduced-
 242 impact logging sites (e.g., Pinagé et al., 2019). Details on site-specific data used in this
 243 study are available in Text S2 and previous work (Longo et al., 2016; Vincent et al., 2017;
 244 Brando, Silvério, et al., 2019), and were obtained through the Paracou Experimental Sta-
 245 tion and the Sustainable Landscapes Brazil data servers (Paracou Portal, 2016; Sustain-
 246 able Landscapes Brazil, 2019; dos-Santos et al., 2019).

247 2.2 Overview of the modeling framework

248 In this study, we used the Ecosystem Demography model, version 2.2 (ED-2.2) (Moorcroft
 249 et al., 2001; Medvigy et al., 2009; Longo, Knox, Medvigy, et al., 2019) to simulate the
 250 impacts of forest structure on energy, water, and carbon cycles. For any point of inter-
 251 est, the ED-2.2 model simulates the forest structure and functional diversity across a land-
 252 scape, and simulates the energy, water, and carbon budgets for multiple canopy envi-
 253 ronments, which represent the forest heterogeneity (Longo, Knox, Medvigy, et al., 2019).
 254 ED-2.2 has been successfully evaluated and used in both short-term and long-term stud-
 255 ies in the Amazon forest (Powell et al., 2013; Zhang et al., 2015; Levine et al., 2016; Longo,
 256 Knox, Levine, et al., 2019). In ED-2.2, the horizontal and vertical heterogeneities of forests
 257 are represented through a hierarchical structure. Each area with the same climate (e.g.,

258 footprint of an eddy covariance tower or a grid cell in a gridded meteorological driver)
259 is called a *polygon*. Each polygon is subdivided into *patches*, which represent collections
260 of forest gaps within a polygon that share a similar age since last disturbance and same
261 disturbance type (although not necessarily contiguous in space). Patches are further sub-
262 divided into *cohorts*, which are collections of individual plants that have similar size and
263 similar functional group. Importantly, because ED-2.2 incorporates the horizontal het-
264 erogeneity of the plant community structure and composition, the model can efficiently
265 incorporate and simulate the dynamics of degraded forests.

266 Most of the ED-2.2 modules used in this study have been previously described in
267 Longo, Knox, Medvigy, et al. (2019). The main changes used in this study include (1)
268 a modified height-diameter allometry based on the Jucker et al. (2017) approach and lo-
269 cally collected field data that can be used consistently by the initialization and model;
270 (2) an improved allocation to living and structural tissues, which is now based on more
271 recent allometric equations (Chave et al., 2014; Falster et al., 2016) and datasets (Falster
272 et al., 2015); (3) a revised photosynthesis solver, which now accounts for the maximum
273 electron transport ratio and the maximum triose-phosphate utilization (von Caemmerer,
274 2000; Oleson et al., 2013; Lombardozzi et al., 2018); (4) updated values of traits that are
275 used to define trade-offs in tropical plant functional types in ED-2.2 (wood density and
276 leaf turnover rate), and updated the trade-off relationships of traits that directly or in-
277 directly influence gross primary productivity and light- and water-use efficiency (specific
278 leaf area and leaf carbon:nitrogen ratio, maximum carboxylation rate, maximum elec-
279 tron transport ratio and maximum triose-phosphate utilization), using multiple studies
280 and trait databases, including GLOPNET, TRY, and NGEETropics (I. J. Wright et al.,
281 2004; Santiago & Wright, 2007; Chave et al., 2009; Kattge et al., 2009, 2011, 2020; Bar-
282 aloto et al., 2010; Powers & Tiffin, 2010; Gu et al., 2016; Bahar et al., 2017; Norby et
283 al., 2017). These changes are described in Text S3. Moreover, we used an approach de-
284 veloped by X. Xu (unpublished) and based on Lloyd et al. (2010) to account for light-
285 dependent plasticity of three leaf traits (specific leaf area, leaf turnover rate, and car-
286 boxylation capacity), and calibrated using existing data (Lloyd et al., 2010; Russo & Ki-
287 tajima, 2016; Keenan & Niinemets, 2016).

288 To obtain initial conditions for ED-2.2 from airborne lidar, we devised a multi-step
289 approach that links airborne lidar data with ecosystem properties (Figure 2). Here we
290 provide a summary of the initialization procedure; the technical details of this approach

291 are described in Text S4. For step 1, we split all collected point cloud data into 50×50 m
292 columns, simulated waveforms from the discrete returns (Blair & Hofton, 1999; Popescu
293 et al., 2011; Hancock et al., 2019) to obtain unscaled leaf area density profiles based on
294 the vertical distribution of returns (e.g., MacArthur & Horn, 1969; Ni-Meister et al., 2001;
295 Stark et al., 2012; Antonarakis et al., 2014; Tang & Dubayah, 2017), and assigned the
296 relative proportion of each plant functional type provided by one of the 769 training plots
297 that had the most similar vertical structure; the similarity was based on the profile com-
298 parison that yielded the smallest Kolmogorov-Smirnov statistic. The vertical profile was
299 split into cohort layers centered around local maxima or saddle points, using a modified
300 procedure based on function `peaks` (package `RSEIS`, Lees, 2017) of the R statistical soft-
301 ware (R Core Team, 2019). For step 2, we used a collection of 817 forest inventory plots
302 (0.16–0.26 ha) that were also surveyed by airborne lidar, which included plots from all
303 study regions as well additional sites available from Sustainable Landscapes Brazil (SLB)
304 and used in a previous study (ancillary SLB sites, Figure 1; Longo et al., 2016); we de-
305 veloped statistical models based on subset selection of regression (A. J. Miller, 1984) and
306 heteroskedastic distribution of residuals (Mascaro et al., 2011) to estimate plot-level prop-
307 erties (aboveground biomass, basal area, stem number density, leaf area index) from point
308 cloud metrics and field estimates, following the approach by Longo et al. (2016). For step
309 3, we sought to obtain a plot-specific scaling factor to the leaf area density profile that
310 produced the best agreement between the four estimated plot-level properties from step
311 1 and the plot-level properties obtained by integrating the vertical distribution from step
312 2, by minimizing the sum of relative square differences of the four properties. For step
313 4, we analyze the scaling factor distribution for all plots for which we could test the ap-
314 proach, and define a unique and global scaling factor, based on the median scaling fac-
315 tor, that is used to correct all predicted profiles.

316 Once we obtained the initial conditions for each 50×50 m column, we grouped in-
317 dividual columns based the disturbance history (degradation level) and the study region
318 (Table 1). We used the following broad categories for disturbance history: intact (INT),
319 reduced-impact logging (RIL), conventional logging (CL_x , where x is the number of log-
320 ging disturbances), conventional logging and thinning (LTH), logged and burned once
321 (LB1) and burned (BN_x , where x is the number of burns). Importantly, we did not per-
322 form any averaging or sampling of the individual columns before providing them to ED-

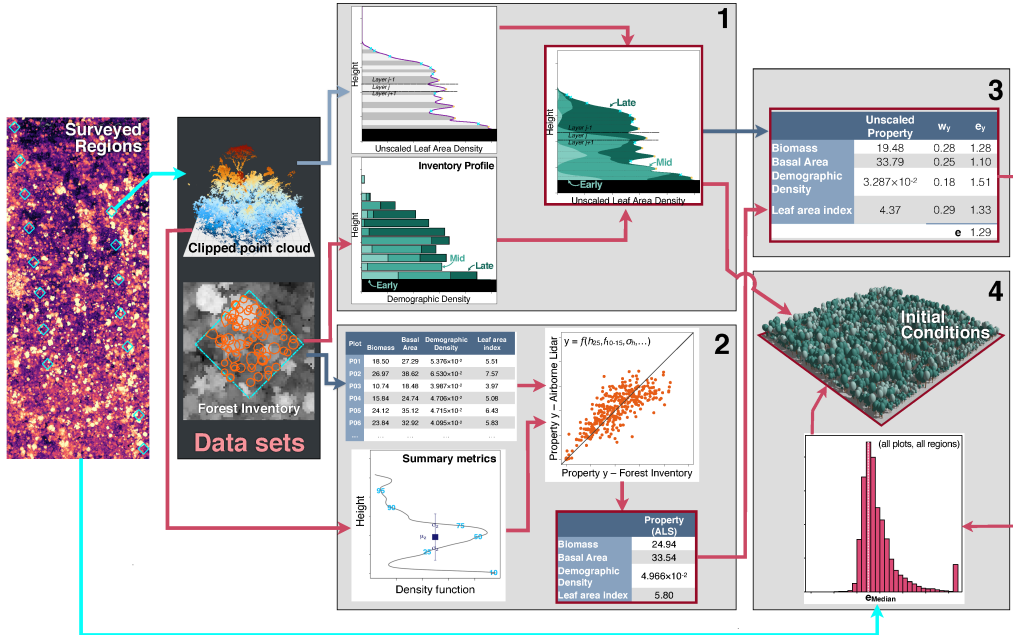


Figure 2. Schematic representation of the method to obtain initial conditions for ED-2 from airborne lidar. Each light box represents one step in the procedure. The results of each step are highlighted with a red border. Dark blue arrows are stages that require individual-based allometric equations, and light blue arrows are stages that require a light extinction model.

2.2; instead, we provided all columns to the model, so the initial conditions characterize the observed distribution of forest structures that exist within each group.

2.3 Assessment of the modeling framework

We evaluated three characteristics to assess the ability of model framework to represent the forest structure heterogeneity caused by degradation, and to represent components of the energy, water, and carbon cycle. First, we quantified the ability of the airborne lidar initialization to capture the differences in forest structure caused by degradation. Second, we assessed whether the model can realistically represent fluxes and storage of water, energy and carbon across different regions. Third, we compared the model sensitivity to degradation-driven effects on fluxes and storage with independent observations.

To evaluate the airborne lidar initialization, we used a cross-validation approach in which we replicated the procedure described above (Section 2.2) 2000 times, using a

336 hierarchical bootstrap approach. We first sampled regions (with replacement), to ensure
337 that some regions would be entirely excluded from the replicate, then we sampled plots
338 (also with replacement), to ensure that the replicate had the same number of plots as
339 the original training data set. We then predicted the structure of all plots in the excluded
340 regions, using iterations that did not have any plot in the training data set; to make this
341 number consistent across regions, we used the smallest number of iterations that met this
342 criterion across all regions ($n = 612$). Finally, for each region, we compared the average
343 forest structure from all cross-validation replicates that excluded the region from the train-
344 ing stage. Because estimates of forest properties have larger uncertainties in smaller plots
345 (Chave et al., 2004; Meyer et al., 2013; Mauya et al., 2015), we only evaluated the method
346 when a disturbance class within a region had at least 20 plots.

347 To verify the model’s ability to realistically represent the regional variability of fluxes
348 and storage, we carried out ED-2.2 simulations initialized with airborne lidar for the in-
349 tact forests regions where eddy covariance tower and forest inventory plots co-located
350 with airborne lidar were available (GYF and BTE). Region TAN had two eddy-covariance
351 towers, one within the footprint of the burned forests and a second in intact forest (Brando,
352 Silvério, et al., 2019), which allowed us to contrast the model’s predicted impacts of degra-
353 dation on fluxes and biophysical properties with the pair of tower measurements.

354 **2.4 Model configuration and analyses**

355 Our main focus is to understand the role of degradation-driven changes in forest
356 structure in altering both the state and the fluxes of energy, water, and carbon, both un-
357 der typical and extreme climate. To account for regional differences in climate and to
358 sample a broad range of interannual variability, we used time series of meteorological drivers
359 pooled from gridded reanalyses (one set of time series per region). For most meteorolo-
360 gical variables required by ED-2.2 (pressure, temperature, humidity, incoming short-
361 wave and longwave radiation, and winds), we used $0.625^\circ \times 0.5^\circ$, hourly averages (1980–
362 2016) from the version 2 of the Modern-Era Retrospective Analysis for Research and Ap-
363 plications (MERRA-2, Gelaro et al., 2017). MERRA-2 precipitation is known to have
364 significant negative biases in the tropics (Beck et al., 2019); therefore we used the $0.1^\circ \times 0.1^\circ$,
365 3-hourly precipitation rates from the version 2 of the Multi-Source Weighted Ensemble
366 Precipitation product (MSWEP-2, Beck et al., 2019). To ensure that the only difference
367 between simulations in the same study region was the distribution of forest structures,

368 we imposed the same edaphic conditions: free-drainage soils with 8 m deep, and nearly
 369 equal fractions of sand (32%), silt (34%), and clay (34%). To avoid confounding effects
 370 from post-disturbance mortality and recovery, all simulations were carried out without
 371 enabling dynamic vegetation, such that the differences in forest structure would remain
 372 the same for the entire time series, and all differences between simulations in the same
 373 region could be attributable to well-characterized differences in forest structure. How-
 374 ever, disabling dynamic vegetation also precluded us from investigating the effects of climate-
 375 driven changes in the canopy structure on the energy, water, and carbon cycle, and thus
 376 potentially increasing biases in our estimates of fluxes following extreme events such as
 377 droughts.

378 To investigate the role of degradation on fire risk, we built on the original fire model
 379 from ED-1 (Moorcroft et al., 2001) to determine when fire-prone conditions would oc-
 380 cur in each patch. The flammable area α_F ($\% \text{ yr}^{-1}$) is calculated from the fire distur-
 381 bance rate λ_F (yr^{-1}):

$$\alpha_F = 100 [1 - \exp(-\lambda_F \Delta t)], \quad (1)$$

$$\lambda_F = \begin{cases} I C_{\text{Fuel}} & , \text{ if } \left[\frac{1}{|z_F|} \int_{z_F}^0 \vartheta(z) dz \right] < (1-f) \vartheta_{\text{WP}} + f \vartheta_{\text{Fc}} \\ 0 & , \text{ otherwise} \end{cases} . \quad (2)$$

382 where $\Delta t = 1 \text{ yr}$; $I = 0.5 \text{ m}^2 \text{ kgC yr}^{-1}$ is a fire intensity parameter; $z_F = 30 \text{ cm}$ is the
 383 depth of the soil layer used to estimate dryness; ϑ ($\text{m}^3 \text{ m}^{-3}$) is the soil moisture; ϑ_{WP}
 384 is the permanent wilting point and ϑ_{Fc} is the field capacity, both defined as in Longo,
 385 Knox, Medvigy, et al. (2019); and $f = 0.02$ is a phenomenological parameter that de-
 386 fines dry conditions. The values of I and f were selected based on the results from a pre-
 387 vious model evaluation using ED-2.2 (Longo, Knox, Levine, et al., 2019). Because un-
 388 derstorey fires are the dominant type of fire in the Amazon (A. Alencar et al., 2006; Mor-
 389 ton et al., 2013), we considered fuels to be comprised by above-ground litter, above-ground
 390 coarse woody debris, and above-ground biomass from grasses and seedlings (trees with
 391 height $< 2 \text{ m}$); canopy trees were not considered to be fuels. The fire parameterization,
 392 although simple, has been previously demonstrated to capture the general features of fire
 393 regime across tropical South America (Longo, Knox, Levine, et al., 2019).

3 Results

3.1 Evaluation of the model initialization and simulated seasonal dynamics

The ED-2.2 model initialization approach from airborne lidar (Figure 3) captured the main differences in forest structure and composition, both across study regions and along degradation gradients. To illustrate the initialization, we focus on the basal area distribution obtained from cross-validation at disturbance histories within study regions that had at least 20 plots (Figure 3). At sites GYF, PRG, and TAN, the airborne lidar initialization predicted the total basal area with absolute biases ranging from 3% (GYF) to 13% (TAN), and root mean square error of the order of 18–27% (Figures 3c, 3f and 3i). The largest absolute discrepancies occurred for intermediate-sized trees ($20 \leq \text{DBH} < 40$ cm) at GYF and PRG, where the airborne lidar initialization underestimated basal area by 2.9 and 4.3 $\text{cm}^2 \text{m}^{-2}$, respectively (Figures 3c and 2f). The largest overestimation of airborne lidar was observed among larger trees ($60 \leq \text{DBH} < 100$ cm) in intact forests at GYF (2.4 $\text{cm}^2 \text{m}^{-2}$; Figure 3c). The size distribution of most degraded forests were well characterized (Figures 3a-b, 3d-e and 3g); the largest deviations from inventory were observed in logged and burned forests in PRG, where airborne lidar underestimated total basal area by 3.0 $\text{cm}^2 \text{m}^{-2}$ (Figure 3d). Likewise, the initialization algorithm represented the higher relative abundance of early successional plants in the most degraded sites, and the dominance of mid- and late-successional plants at intact forests at GYF and PRG (Figure S1), and realistically represented the leaf area distribution across regions and degradation levels (Figure S2).

ED-2.2 simulations using forest inventory and airborne lidar as initial conditions were compared with eddy covariance tower estimates of all sites (Figures 4 and S4-S9, and Table S1). Gross primary productivity (GPP) generally showed small biases relative to tower estimates (-0.046 to $+0.394 \text{ kgC m}^{-2} \text{ yr}^{-1}$), and relatively small errors (less than observed variability) at all sites, regardless of the initial conditions (Figure 4; Table S1). While the GPP seasonality was correctly represented at GYF, the model did not capture the late wet-season decrease and early dry-season increase of GPP at BTE, and it showed a delayed dry-season decline GPP at TAN compared to tower estimates (Figure S4). Net ecosystem productivity (NEP), on the other hand, showed significant biases, large errors, and relatively small correlation with tower estimates (Figure 4; Ta-

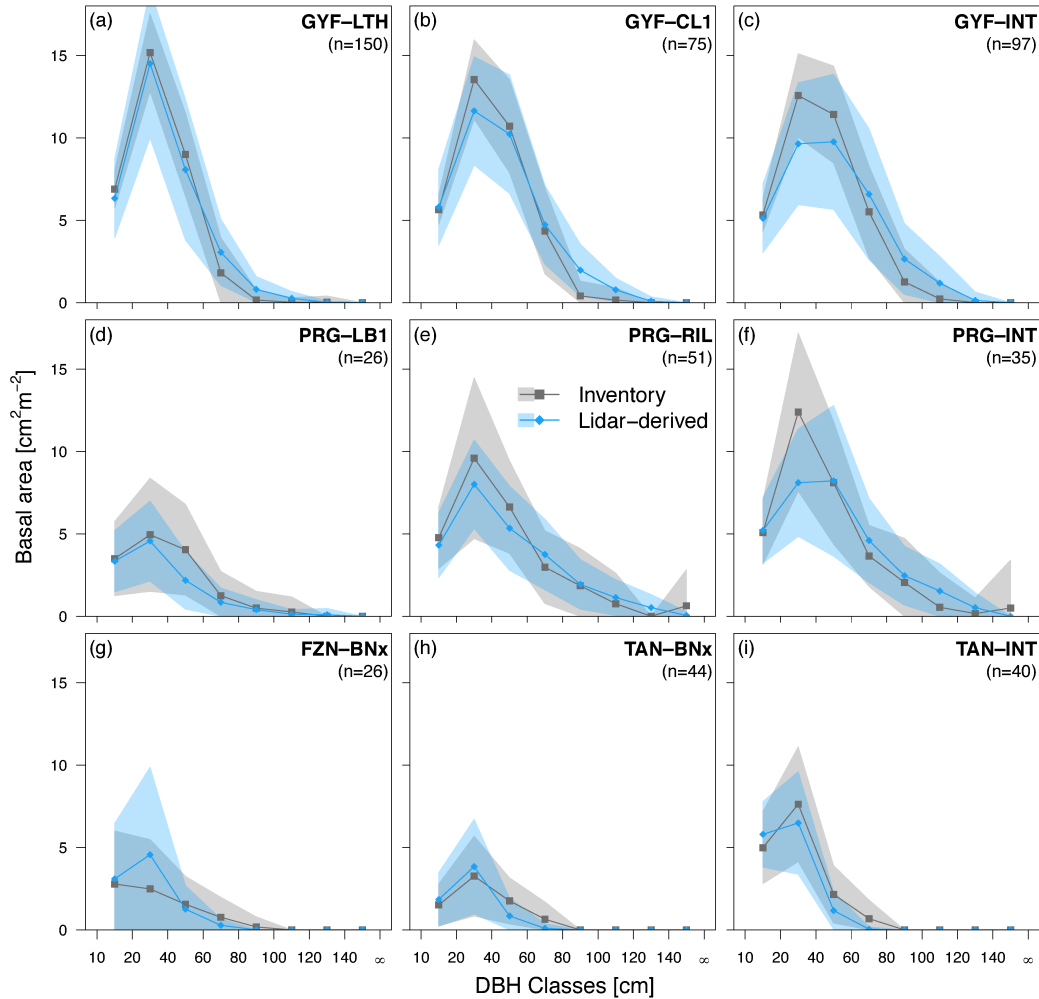


Figure 3. Assessment of basal area distribution as a function of diameter at breast height (DBH) for different study regions and degradation levels. Grey points are obtained from forest inventory plots, and blue points are obtained from the airborne lidar initialization (Figure 2) using a 612-fold regional cross-validation (i.e. excluding all plots from region in the calibration stage). Bands around points correspond to the standard deviation either across all plots in the same category (inventory) or across all plots and replicates (lidar). Sites: GYF – Paracou, PRG – Paragominas, FZN – Feliz Natal, TAN – Tanguro. Disturbance classes: BNx – Burned twice or more, CL1 – conventional logging (once), LB1 – logged and burned once, LTH – logged and thinned, RIL – reduced-impact logging, INT – intact. Additional comparisons are shown in the Supporting Information: basal area as functions of plant functional type (Figure S1); leaf area index profiles as functions of height (Figure S2); comparisons for Belterra (BTE-RIL) (Figure S3).

426 ble S1), which were driven by excessive seasonality of heterotrophic respiration (Figure S5).
427 Because the initial carbon stocks in necromass pools are uncertain, and the results on
428 magnitude and seasonality of ecosystem respiration (and consequently NEP) are incon-
429 sistent with tower estimates, we will not discuss the simulation results in terms of res-
430 piration and NEP.

431 Water fluxes also showed small biases relative to the observed variability at GYF,
432 TNF and TAN (Burned), regardless of the initialization (-0.01 to $+0.54$ mm day $^{-1}$; Fig-
433 ures 4a and 4c; Table S1); biases at TAN (Intact) were larger ($0.69-0.82$ mm day $^{-1}$).
434 With the exception of TAN (Burned), the correlation between ED-2.2 and tower was high
435 at daily averages (Figures 4b and 4d; Table S1). At TAN (Burned), the poorer agree-
436 ment with tower estimates was caused by the model predicting a similar seasonality of
437 water flux at both control and burned forests, whereas towers suggest an increase in wa-
438 ter flux during the earlier part of the dry season (Figure S6). ED-2.2 predictions of sen-
439 sible heat flux had high correlation with observations at all sites (Figures 4b and 4d; Ta-
440 ble S1), although sensible heat flux shows significant biases at BTE, and dampened sea-
441 sonality at GYF and TAN (Burned) (Figures 4a and 4c; Table S1; Figure S6). Outgo-
442 ing shortwave radiation correctly captured the seasonality at the wettest sites, but it did
443 not capture the sharp dry-season increase at TAN (Figure S8), which may be associated
444 with dry-season leaf senescence and shedding that was likely underestimated by ED-2.2.
445 In addition, ED-2.2 simulations overestimated outgoing longwave radiation at all sites
446 except at TAN (Burned) using inventory initialization (Figure S9). Nonetheless, the sea-
447 sonality and the intra-seasonal variation of outgoing longwave radiation were correctly
448 captured by ED-2.2, resulting in generally high correlation and small standard devia-
449 tion of residuals at most sites (Figure 4; Table S1).

450 **3.2 Degradation effects on seasonality of fluxes**

451 From ED-2.2, we found that forest degradation can have substantial impacts on
452 the ecosystem function such as evapotranspiration (ET) or ground temperature in severely
453 or recently degraded forests, and in parts of the Amazon with a longer dry season. At
454 GYF, the airborne lidar survey sampled only intact forests and areas that were logged
455 25 years prior to the data acquisition: consequently, the average water vapor flux and
456 ground temperature were nearly indistinguishable across degraded and intact forests (Fig-
457 ures 5a,S10a). At the equatorial sites, degradation effects were small during the wet sea-

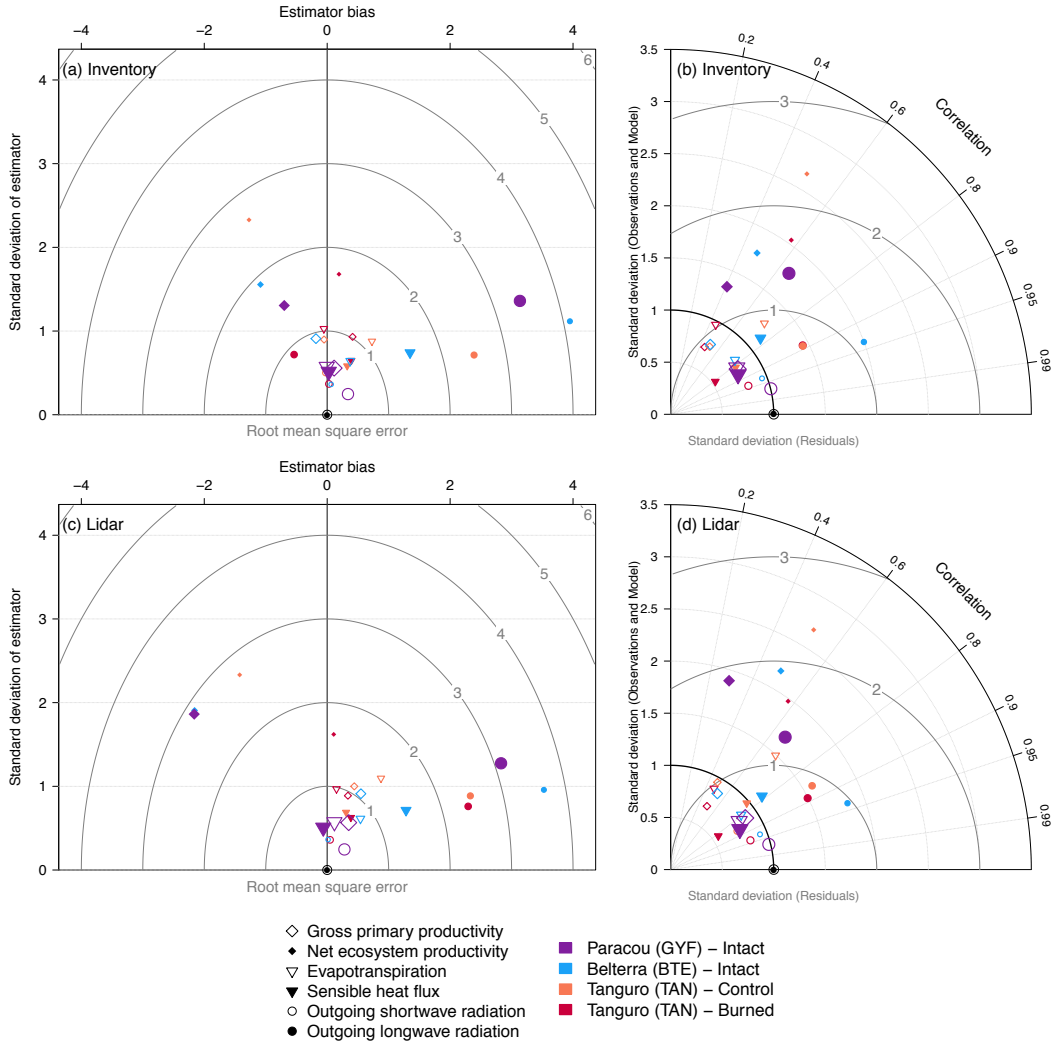


Figure 4. Summary of ED-2.2 model assessment using eddy covariance towers as benchmarks, using simulations initialized with forest inventory and airborne lidar. (a,c) Bias-variance diagram and (b,d) Taylor diagram of multiple daily-averaged fluxes of carbon, energy, and water for Paracou (GYF), Belterra (BTE) and Tanguro (TAN, control and burned), for simulations initialized with (a,b) forest inventory plots and (c,d) airborne lidar. In the bias-variance diagram, bias (x axis), standard deviation of residuals (y axis) and root mean square error (concentric arcs) are normalized by the standard deviation of observations, as is the standard deviation of models in the Taylor diagram. In both diagrams, \odot corresponds to the perfect model prediction. In all plots, we only compare daily averages of days with no measurement gaps. Comparisons of the seasonal cycle for all variables included in the diagrams are available at Figures S4-S9.

458 son but showed marked reduction in ET (2.1–6.7% in BTE and 4.3–31.8% in PRG) and
459 increase in daytime temperature (0.4–0.9°C in BTE and 1.0–6.0°C in PRG) during the
460 dry season, with the largest changes relative to intact forests found at burned areas (Fig-
461 ures 5b, 5c, S10b,c). At the southern (driest) sites, the seasonal changes were even more
462 pronounced: at both FZN and TAN, ET decreased by 21–25% early in the dry season
463 (Jun) at the most severely burned forests, whereas ET in intact forests peaked in the mid-
464 dle of the dry season (Jul–Aug; Figures 5d and 5e). Similarly, burned forests were warmer
465 year-round than intact forests at the southern sites (FZN and TAN), with minimum warm-
466 ing during the wet season (Dec–Mar; 0.5–0.8°C), and maximum warming occurring at
467 the peak of the dry season (Jul–Aug; 1.0–6.5°C; Figures S10d and S10e).

468 Importantly, the ED-2.2 results in Figures 5 and S10 emerge from the different dis-
469 tribution of forest structures associated with degradation histories. ED-2.2 accounts for
470 the diversity of forest structures within each disturbance history by means of patches;
471 each patch represents a different forest structure found within any disturbance regime,
472 and patch area is proportional to the probability of finding such forest structure (Longo,
473 Knox, Medvigy, et al., 2019). For example, the ground temperature is consistently warmer
474 at the low biomass patches, but the differences between the lowest and highest patch tem-
475 peratures are as low as 1°C at GYF (Figure 6a) and less than 4°C during the wet sea-
476 son even at the southern regions (Figures 6d and 6e). In contrast, differences along biomass
477 gradients exceed 9°C during the dry season at all regions except GYF (Figure 6).

478 Likewise, when all simulated patches are considered, we observe strong coherence
479 between biomass and gross primary productivity (GPP) across all regions and through-
480 out the year (Figures 7 and S11). However, the effect of local communities on GPP is
481 seasonal: differences in typical GPP between low-biomass and high-biomass patches do
482 not exceed $1.1 \text{ kgC m}^{-2} \text{ yr}^{-1}$ during the wettest months (Figures 7a–7c), whereas the range
483 of GPP reaches $0.7 \text{ kgC m}^{-2} \text{ yr}^{-1}$ at the short dry-season at GYF and exceeds $2.0 \text{ kgC m}^{-2} \text{ yr}^{-1}$
484 during the dry season at the most degraded and driest sites (Figures 7e and 7f). Sim-
485 ilar effects were observed in evapotranspiration, where differences along biomass are the
486 strongest during the dry season (Figure S12).

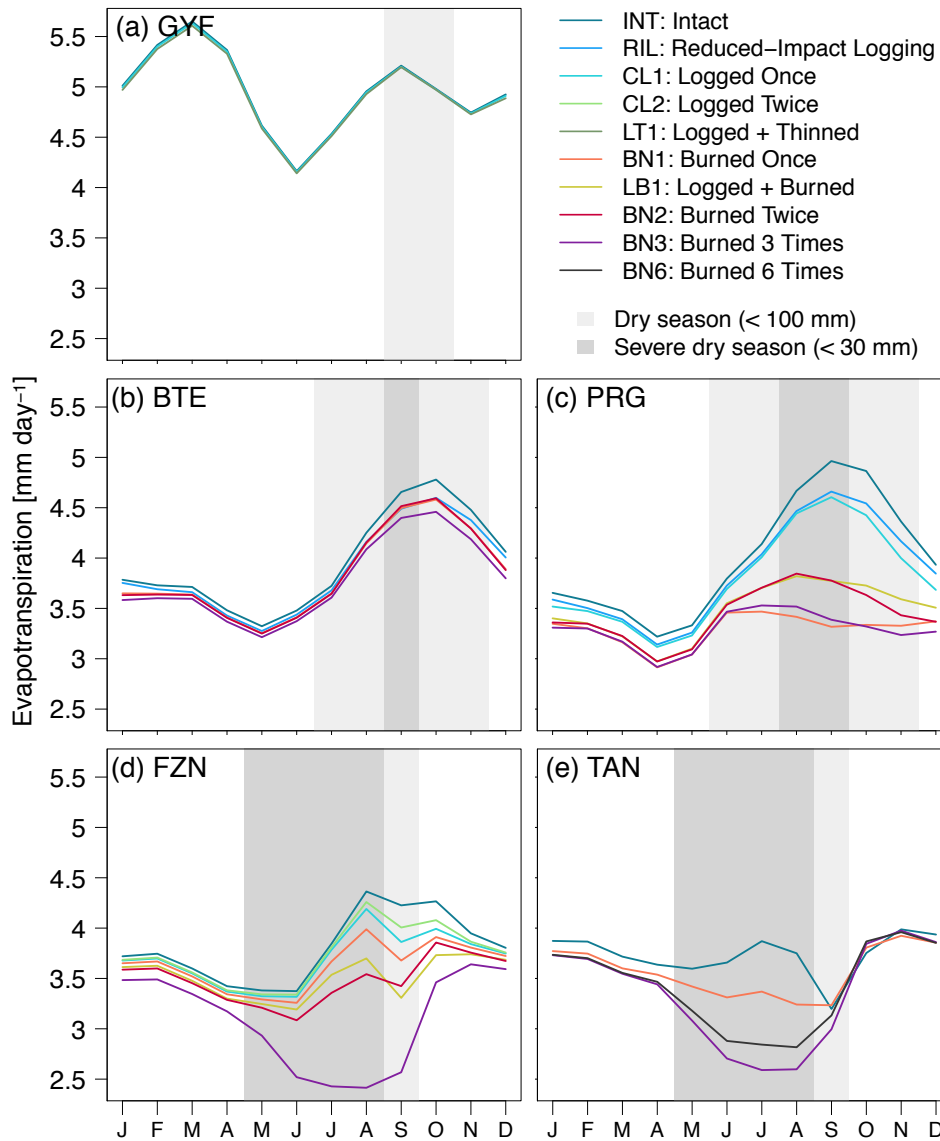


Figure 5. Monthly mean evapotranspiration (ET) as a function of region and degradation. Monthly averages correspond to the 1980–2016 period, simulated by ED-2.2 for (a) Paracou (GYF), (b) Belterra (BTE), (c) Paragominas (PRG), (d) Feliz Natal (FZN), and (e) Tanguro (TAN), aggregated by degradation history within each region (lines). Grey rectangles in the background correspond to the average dry season.

487

3.3 Degradation impacts on forest flammability

488

The impact of forest degradation on ecosystem functioning showed important year-to-year variability, and differences between intact and degraded forests were generally

489

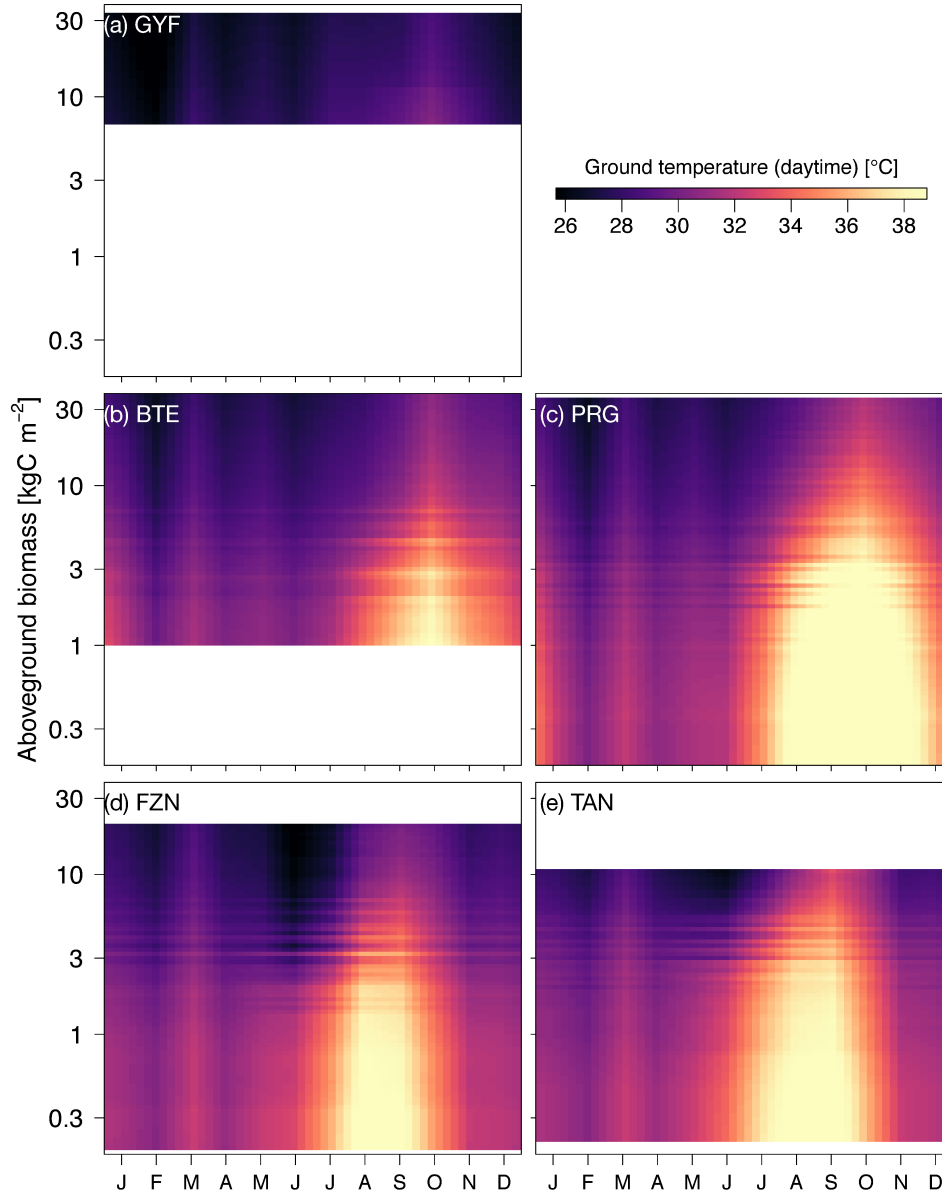


Figure 6. Monthly mean daytime ground temperature as a function of region and local (patch) aboveground biomass. Monthly averages correspond to the 1980–2016 period, simulated by ED-2.2 for (a) Paracou (GYF), (b) Belterra (BTE), (c) Paragominas (PRG), (d) Feliz Natal (FZN), and (e) Tanguro (TAN), and the y axis corresponds to the aboveground biomass for each patch, linearly interpolated for visualization. White areas are outside the range of biomass of each region and thus excluded.

490 larger during typical years than during extreme droughts. For this section, we calculate
 491 the monthly water deficit based on the difference between potential evapotranspiration

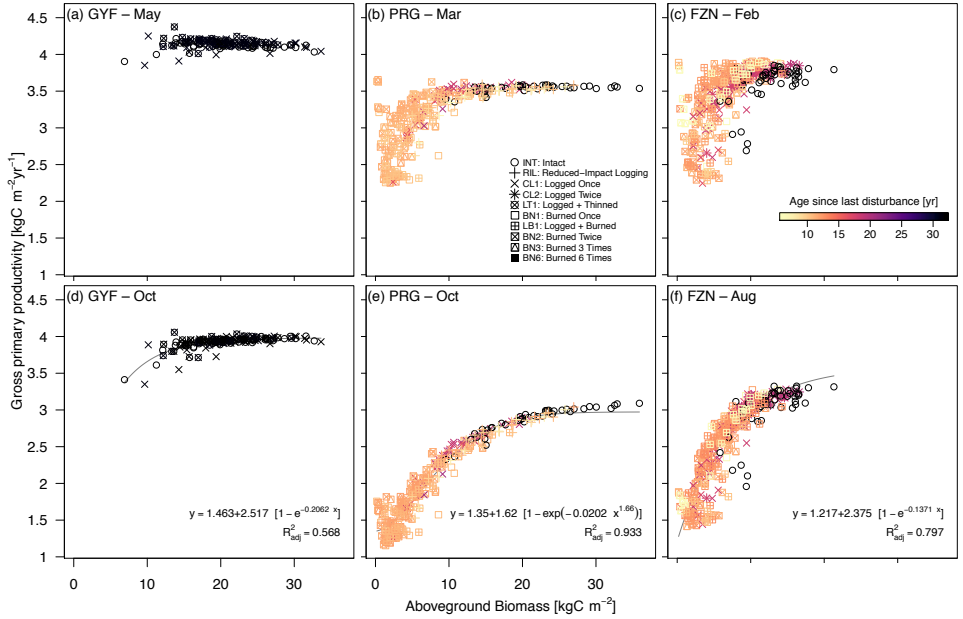


Figure 7. Variability of gross primary productivity (GPP) as a function of local (patch) aboveground biomass (AGB). Scatter plot of AGB (x axis) and GPP (y axis) at sites (a,d) Paracou (GYF), (b,e) Paragominas (PRG), (c,f) Feliz Natal (FZN), for (a-c) the peak of wet season — May (GYF), March (PRG), and February (FZN) — and (d-f) peak of dry season — October (GYF and PRG), and August (FZN). Each point represents the 1980–2016 average GPP of each patch solved by ED-2.2; point shapes correspond to the disturbance history, and point colors represent the time between the last disturbance (undetermined for intact forests) and lidar data acquisition. Curves correspond to non-linear least squares fits of the most parsimonious function, defined from Bayesian Information Criterion (Schwarz, 1978), between shifted exponential or shifted Weibull functions. Only fits that produced $R_{adj}^2 > 0.5$ were included.

492 (calculated following Priestley & Taylor, 1972) and rainfall, and relate the 12-month run-
 493 ning averages of multiple response variables with the maximum cumulative water deficit
 494 over the previous 12 months, and define drought length as the number of consecutive months
 495 in water deficit exceeds 20 mm. Using region PRG as an example, as the region has the
 496 broadest range of recent disturbances and maximum cumulative water deficit, we found
 497 that, during typical rainfall periods, evapotranspiration in logged forests and burned forests
 498 were 3–6% and 11–22% lower than intact forests, respectively (Figure 8a); this differ-
 499 ence was significantly reduced or even reversed during severe droughts, when evapotran-
 500 spiration of degraded forests were up to 4% higher than in intact forests (Figure 8a). De-

501 graded forests have a lower proportion of shade-tolerant, late-successional trees, and typ-
502 ical stomatal conductance is higher by 19–34% in burned forests and by 5–13% in logged
503 forests (Figure 8b). This result indicates that the reduced typical evapotranspiration re-
504 sults from degraded forests having lower leaf area index relative to intact forests, as lo-
505 cal leaf area index is related to local aboveground biomass (Figure S13). In addition, ex-
506 treme droughts did not substantially reduce the differences in stomatal conductance be-
507 tween degraded and intact forests (Figure 8b). While evapotranspiration was generally
508 lower in degraded forests, total evaporation (from ground and canopy intercepted wa-
509 ter) was higher in most degraded forests, with burned forests experiencing 3–26% more
510 evaporation in typical years and 0–14% during severe droughts (Figure 8c). The com-
511 bination of higher evaporation and relatively shorter canopy (shallower roots) in degraded
512 forests were typically translated into slightly drier near-surface soils (Figure 8d): dur-
513 ing typical years, soil water availability at the top 30 cm layers was 1.2–12% lower in burned
514 forests than intact forests, whereas the differences were more modest in logged forests
515 (0.2–3%) and even reversed during extreme droughts (Figure 8d). Carbon and energy
516 fluxes showed similar behavior. Gross primary productivity in intact forests steadily de-
517 creased with increased drought severity, and the depletion of productivity caused by degra-
518 dation is most marked during typical years but is reduced during severe droughts (Fig-
519 ure S14a). While ground temperature is always higher in degraded forests (Figure S14b),
520 differences in sensible heat fluxes and outgoing longwave radiation also diminish during
521 extreme drought conditions (Figure S14c,d).

522 Degraded forests show drier near-surface soils (Figure 8d) and warmer surface tem-
523 peratures (Figure S14) than intact forests for most years, yet the interannual variabil-
524 ity of climate also modulates the differences in water, carbon, and energy cycles between
525 degraded and intact forests (Figures 8 and S14). Therefore, both degradation and cli-
526 mate may influence the flammability of forests. The average flammable area predicted
527 by ED-2.2 (Section 2.4) shows large variation across regions, ranging from nearly zero
528 at GYF forests (the wettest region) to over $25\% \text{ yr}^{-1}$ at some of the forests in TAN (the
529 driest region) (Figure 9a). Within each region (i.e. under the same prescribed climate),
530 the model generally predicted higher flammability for the shortest forests ($< 10 \text{ m}$), al-
531 though predictions also indicate large within-region variability of flammable area for forests
532 with intermediate canopy height (10–25 m) (Figure 9a). For most forests, flammable con-
533 ditions were predicted mostly during moderate or severe droughts, regardless of the degra-

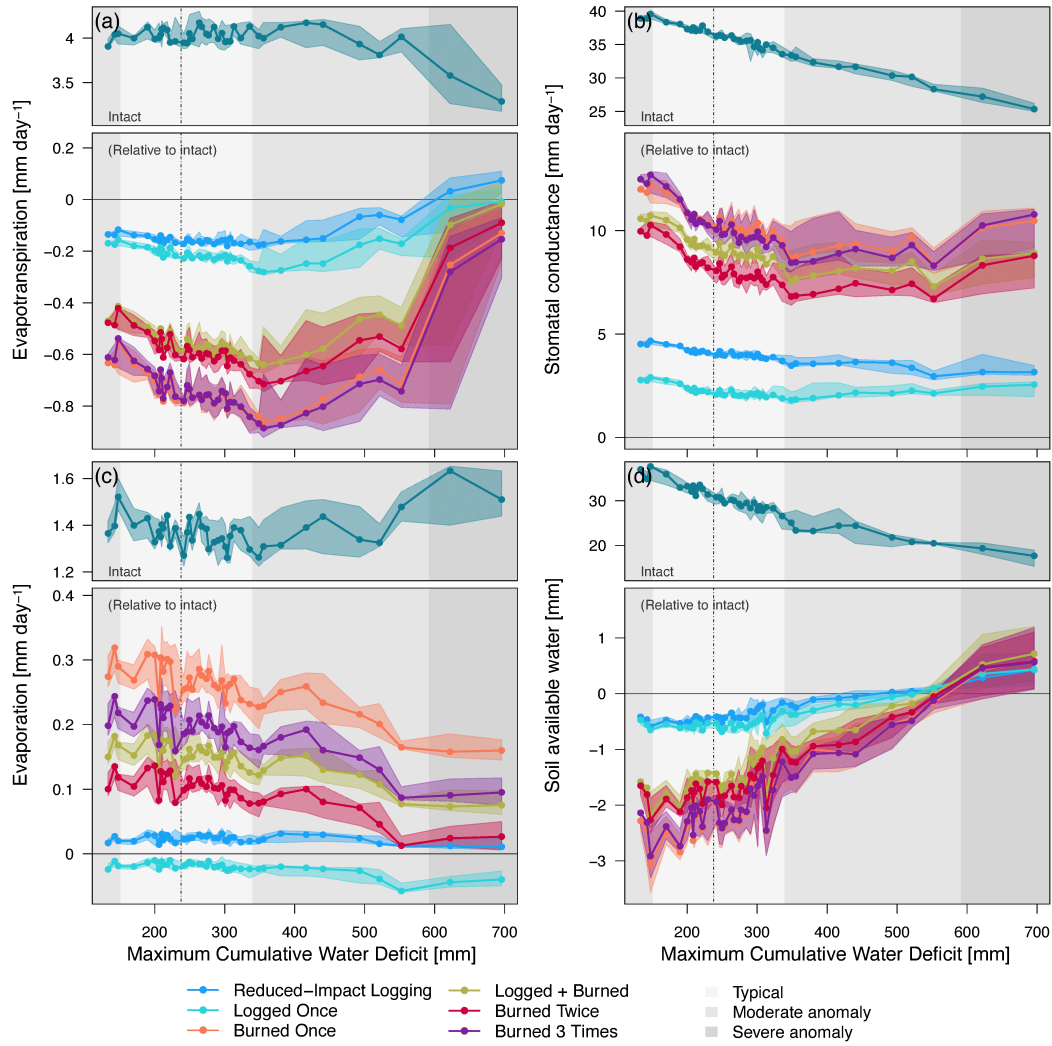


Figure 8. Response of the water cycle components across a forest degradation gradient and drought severity in Paragominas (PRG). Selected components: (a) Total water vapor flux, (b) stomatal conductance, averaged by leaf area, (c) evaporation, and (d) soil available water (i.e. in excess of permanent wilting point) of the top 30 cm. Points correspond to the median value of 12-month running averages, aggregated into 40 quantiles along the range of maximum cumulative water deficit (MCWD). Bands around the points correspond to the 95% range within each MCWD bin. Top panels are the absolute value for intact forests, and bottom panels are the absolute difference between degraded and intact forests. Background shades denote the MCWD anomaly: light gray – 68% range around the median (dot-dash vertical line); intermediate gray – 95% range; dark gray – anomalies exceeding the 95% range.

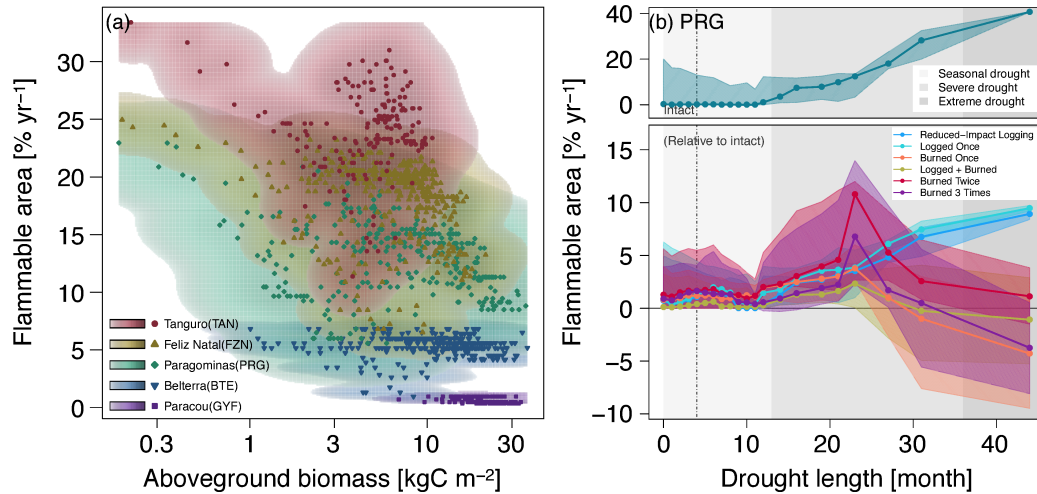


Figure 9. Average flammability as functions of degradation and climate variability. (a) Scatter plot shows the average flammable area (1980–2016) for each simulated patch across all regions, as a function of canopy height. Density cloud (background color) was produced through a bi-dimensional kernel density estimator; points are the averages used to generate each density cloud. Color ramps (logarithmic) range from 0.1 – 100% of the maximum computed scale. (b) Flammable area at region PRG, as a function of degradation history and drought length (number of consecutive months with water deficit in excess of 20 mm). Points correspond to the median value of 12-month running averages, aggregated into quantiles along the drought length. Bands around the points correspond to the 95% range within each drought length bin. Top panels are the absolute value for intact forests, and bottom panels are the absolute difference between degraded and intact forests. Background shades denote drought-length classes used in the text: seasonal (light gray, less than 12 months); severe (intermediate gray, 12–36 months); extreme (dark gray; more than 36 months). Flammability response to degradation and drought duration for other regions are shown in Figure S15.

534 degradation history, as exemplified by region PRG (Figure 9b). While the time series of flammable
 535 area were synchronized across degradation types, ED-2.2 predictions of flammable area
 536 were generally higher for burned forests than intact or lightly logged forests (Figures 9b
 537 and S15). The one exception was the driest region (TAN), where forests that burned mul-
 538 tiple times experienced lower flammability than intact forests (Figure S15d); at TAN,
 539 even intact forests were relatively short (Figure 9a), which caused ED-2.2 to predict lim-
 540 ited access to deeper soils and increased desiccation.

4 Discussion

4.1 Initialization of forest structure from remote sensing

Our method to derive the vertical structure of the canopy from high-resolution airborne lidar successfully characterized the diversity of forest structures of the Amazon, captured differences in forest structure variability along a precipitation gradient, and described the within-region variability in forest structure caused by forest degradation (Figures 3 and S2-S3). Previous studies have used forest structure derived from remote-sensing data to initialize vegetation demography models in tropical forests (e.g., Hurtt et al., 2004; Antonarakis et al., 2011; Rödiger et al., 2018). However, these studies often assume a relationship between forest structure and canopy height with stand age. While this assumption has been successfully applied to intact and second-growth tropical forests (Hurtt et al., 2004; Antonarakis et al., 2011), the association between forest structure and succession is unlikely to be preserved in degraded forests. For example, understory fires proportionally kill more smaller trees than large trees (Uhl & Kauffman, 1990; Brando et al., 2012; Silva et al., 2018), and selective logging creates complex mosaics of forest structure, with substantial losses of large trees from harvesting, and extensive damage to smaller trees in skid trails (Feldpausch et al., 2005). In contrast, our approach accounts for the entire vertical profile at local (50-m) scale, similarly to Antonarakis et al. (2014), which does not require any assumption on the successional stage of the forest. Importantly, our approach requires only the vertical distribution of returns, and could be adapted to large-footprint, airborne or spaceborne lidar data, including the NASA's Global Ecosystem Dynamics Investigation (GEDI, Hancock et al., 2019).

We demonstrated that the initialization from airborne lidar profiles captures most of the variability across and within regions, yet it has important assumptions and limitations. First, our approach relies on allometric equations to determine both the diameter at breast height (DBH), and the individual leaf area (L_i , Text S4.3), with the implicit assumption, that the contribution of branches, twigs, and stems to the lidar return signal is negligible. In reality, allometric equations have either large uncertainties (DBH) or limited number of samples (Figure S16). Previous studies using destructive sampling and terrestrial laser scanning suggest that wood area index may constitute 7–15% of the plant area index (Olivas et al., 2013; Schneider et al., 2019). The use of allometric equations that account for regional variation (e.g., Feldpausch et al., 2011, 2012), and the ex-

573 pansion of open-source databases, such as the Biomass And Allometry Database (BAAD,
574 Falster et al., 2015) used in our study, could further improve the characterization of the
575 vertical structure. In addition, the increased availability of terrestrial laser scanning (TLS)
576 and high-resolution, low-altitude unmanned aerial vehicle lidar could substantially in-
577 crease the data availability and thus improve the overall quality of allometric equations
578 and constrain the relative contribution of woody tissues to the total plant area (Calders
579 et al., 2015; Stovall et al., 2018; Schneider et al., 2019). Alternatively, techniques that
580 extract individual tree crowns from lidar point clouds readily provide highly accurate
581 local stem density and local size-frequency distributions (e.g., tree height or crown size;
582 Ferraz et al., 2016, 2020). These distributions can be used to attribute DBH to individ-
583 uals and generate initial conditions akin to forest inventory to the ED-2.2 model, and
584 data-model fusion techniques that leverage the growing availability of data could reduce
585 uncertainties on many model parameters, including allometry (F. J. Fischer et al., 2019).
586 Finally, ED-2.2 overestimated the seasonality of gross primary productivity and evap-
587 otranspiration at the driest region (TAN) (Figures S4 and S6). This result suggests that
588 simulated rooting depth for TAN was underestimated in the model. Rooting profiles in
589 tropical forests remain largely uncertain: some site studies have sought to relate indi-
590 vidual tree size with rooting depth using isotopic measurements (e.g., Stahl et al., 2013;
591 Brum et al., 2019), whereas regional studies that provide spatial distribution of rooting
592 depth still show important discrepancies in the tropics (e.g., Yang et al., 2016; Fan et
593 al., 2017). Constraining the below-ground allocation of tropical ecosystems should be
594 a priority in future studies.

595 In our study we inferred the functional diversity from forest structure obtained from
596 existing forest inventory plots. The functional group attribution captured the general
597 characteristics of functional composition along degradation gradients (Figure S1), includ-
598 ing the more frequent occurrence of early-successional individuals in degraded forests,
599 consistent with field-based studies (Both et al., 2019); nonetheless, uncertainties in func-
600 tional attribution from field measurements are high. The increased availability of coor-
601 dinated airborne laser scanning (ALS) and airborne imaging spectroscopy (AIS) data
602 in mid-latitudes has lead to opportunities to link structural variability with functional
603 diversity (e.g., Antonarakis et al., 2014; Schneider et al., 2017), and previous studies have
604 successfully integrated ALS and AIS data to attribute functional groups in the ED-2 model
605 (e.g., Antonarakis et al., 2014; Bogan et al., 2019). Overlapping ALS and AIS data over

606 tropical forests are becoming increasingly common (Asner et al., 2014; de Almeida et al.,
607 2019; Laybros et al., 2019) and could provide new opportunities to reduce uncertainties
608 in functional attribution in future studies. Likewise, ongoing and upcoming spaceborne
609 missions at the International Space Station such as GEDI (Hancock et al., 2019), and
610 the Hyperspectral Imaging Suite (HISUI, Matsunaga et al., 2017) will allow for large-
611 scale characterization of structure and function of ecosystems at global scale (Stavros
612 et al., 2017; Schimel et al., 2019).

613 **4.2 Degradation impacts on ecosystem functioning**

614 In addition to carbon losses and structural changes, degradation has substantial
615 impacts on energy and water cycles in Amazonian forests, especially in severely degraded
616 forests with marked dry season. According to the ED-2.2 simulations, ground temper-
617 ature of logged forests ranged from nearly-identical to intact forests (low-impact logging
618 or old logging disturbances) to 0.7°C warmer (recently logged forests), whereas severely
619 burned forests experienced daytime near-surface temperatures increases of as much as
620 4°C (Figure S10), and differences between the lowest and highest biomass patches ex-
621 ceeded 9°C (Figure 6). Observed differences in understory temperatures show large vari-
622 ability, but they generally agree with the ED-2.2 results. For example, results of tem-
623 perature differences between logged and intact areas in the wet forests of Sabah, Malaysia,
624 ranged from negligible to 1.2°C for average maximum temperature (Senior et al., 2018;
625 Jucker et al., 2018). The predicted warmer daytime understory temperatures at recur-
626 rently burned forests also yielded drier near-surface conditions: daytime ground vapor
627 pressure deficit was on average 15–25 hPa greater than in intact forests (equivalent to
628 5–15% reduction in relative humidity), which is within the range observed after the most
629 damaging experimental fire at TAN in 2007 (Brando et al., 2014), and similar to differ-
630 ences in understory relative humidity reported in the dry season between open-canopy
631 seasonally flooded forests and closed-canopy upland forests in the Central Amazon (de
632 Resende et al., 2014). Because temperatures are higher in degraded forests, the simu-
633 lated changes in energy and water cycle caused by degradation also point to a reduction
634 of entropy production in degraded forests, which is consistent with the results across pas-
635 tures and intact forests across the Amazon (Holdaway et al., 2010).

636 ED-2.2 showed various degrees of agreement with the few existing observational
637 studies comparing changes in evapotranspiration due to degradation. Evapotranspira-

tion response to reduced-impact logging was minor (-1.9% reduction relative to intact
in BTE), consistent with eddy covariance tower estimates in a logging experiment in the
same region (-3.7% reduction after accounting for site differences and interannual vari-
ability, S. D. Miller et al., 2011). The model results for the experimental fire at TAN,
however, suggested similar wet-season ET between burned and intact forests ($\Delta ET =$
 $ET_{\text{Brn}} - ET_{\text{Int}} = 0.002 \text{ mm day}^{-1}$), with stronger depletion of ET in burned forests
during the dry season ($\Delta ET = -0.31 \text{ mm day}^{-1}$) (Figures 5 and S6). In contrast, Brando,
Silvério, et al. (2019) found higher ET in burned forests over a period of 4 years, albeit
 ΔET also showed significant interannual variability. A few other studies suggest that the
significant decline in dry-season ET in burned forests may be expected in some areas:
for example, Hirano et al. (2015) found that evapotranspiration of drained and burned
peatlands with second-growth vegetation in Central Kalimantan (Indonesia) was 0.43 mm day^{-1}
lower than drained forests; Quesada et al. (2004) inferred ET changes from soil water
budget in savannas and found significant reductions following fires in a savanna site in
Central Brazil. The advent of high-resolution remote sensing products that quantify en-
ergy, water, and carbon fluxes, such as the ECOSystem Spaceborne Thermal Radiome-
ter Experiment on Space Station (ECOSTRESS) and the Orbiting Carbon Observatory
3 (OCO-3), will provide new opportunities to quantify the role of tropical forest degra-
dation on ecosystem functioning at regional scale (Schimel et al., 2019), as well as to pro-
vide new benchmark data for ecosystem models.

Our model results indicate that severe degradation substantially alters the mag-
nitude and seasonality of energy, water, and carbon fluxes (Figures 5-7 and S10-S12).
In our study, we disabled the vegetation dynamics in ED-2.2 to ensure that predicted
differences in ecosystem functioning could be unequivocally attributed to structural di-
versity, but the differences in ecosystem functioning between degraded and intact forests
may diminish over time as the forest recovers from previous disturbance. This pathway
is consistent with the relatively small differences in ET and surface temperature (Fig-
ures 5-6) observed at logged forests at GYF (25 years since last disturbance) and burned
forests at BTE (15 years since last disturbance). However, the recovery trajectory is one
out of multiple possible pathways: degraded forests may be more prone to subsequent
disturbances (Silvério et al., 2019; Hérault & Piponiot, 2018); the recovery dynamics can
be long or not attainable if multiple stable states exist or if succession is arrested (Mesquita
et al., 2015; Ghazoul & Chazdon, 2017), potentially prolonging the impacts of forest degra-

671 dation on energy and water cycles; and feedbacks on precipitation caused by degrada-
672 tion could affect the spatial distribution of rainfall similarly to the effect observed with
673 deforestation (Spracklen et al., 2018), although to our knowledge this impact has not yet
674 been quantified for degraded forests.

675 In this study, we focused on the effects of forest structure on ecosystem function,
676 and thus we used idealized, homogeneous soil with intermediate hydraulic characteris-
677 tics in all simulations. In reality, soils across the Amazon are highly heterogeneous and
678 directly affect forest structure across the biome (Quesada et al., 2012). Likewise, soil depth
679 and texture and variability in local topography also modulate the effects of tropical for-
680 est degradation on microclimate (Jucker et al., 2018). A previous study using ED-2.2
681 found that evapotranspiration in Central Amazonia could decrease by 12–16% under sce-
682 narios of recurrent yearlong droughts (40% reduction in rainfall), but the severity of the
683 decrease varied by 7% under the same climate scenarios but different soil hydraulic prop-
684 erties (Longo et al., 2018). These results suggest that degraded forests in clay-rich, com-
685 pact soils and deeper water table could amplify reductions in evapotranspiration and gross
686 primary productivity during the dry season, while degradation effects on energy, water,
687 and carbon cycle would likely be dampened in regions where the water table is near the
688 surface for most of the year, or soils with higher water storage capacity.

689 **4.3 Interactions between forest degradation and climate variability**

690 The predicted reductions in evapotranspiration (ET) in the most degraded areas
691 during the dry season suggest that land-use change impacts on the water cycle may be
692 more widespread and pervasive than indicated by earlier studies. Previous model-based
693 studies showed that biome-wide deforestation could cause ET to decrease by 25–40% rel-
694 ative to intact forests in the Amazon during the dry season (e.g., von Randow et al., 2004;
695 Zemp et al., 2017). These reductions are comparable to the ET reductions predicted by
696 ED-2.2 at the most degraded forests (21–32%, Figure 5). Because tropical forest degra-
697 dation affects an area comparable to deforestation in the Amazon (Tyukavina et al., 2017),
698 it may further reduce the strength of the Amazon water vapor source to the atmosphere.
699 In our study, we focused on understanding how climate and structure variability impacts
700 the water and energy fluxes, but degradation-driven changes in these fluxes are likely to
701 feed back into the atmosphere. For example, changes in evapotranspiration and sensi-
702 ble heat flux associated with deforestation are known to either redistribute or reduce to-

703 tal rainfall in tropical forests (Spracklen et al., 2018, and references therein), and a sub-
704 substantial fraction of South American precipitation water comes from evapotranspiration
705 from Amazonian forests (van der Ent et al., 2010). Recent estimates of ET for the Ama-
706 zon Basin from the Gravity Recovery and Climate Experiment (GRACE) suggest that
707 the basin-wide ET (including intact forests) has decreased by 1.7% between 2002 and
708 2015 (Swann & Koven, 2017). In addition, several studies suggest that the dry season
709 in the Amazon is becoming longer (Fu et al., 2013; Sena et al., 2018), and land use change
710 is one of the main drivers of the drying trend (Barkhordarian et al., 2018). The role of
711 forest degradation on ongoing and future changes in climate across the Amazon remains
712 uncertain and deserves further investigation, potentially with coupled biosphere-atmosphere
713 models that represent heterogeneity in forest structure and functioning (Swann et al.,
714 2015; Knox et al., 2015; Wu et al., 2017). Likewise, we could not account for cascading
715 effects of climate on the energy, water, and carbon cycle in this study because we dis-
716 abled dynamic vegetation. However, severe droughts are known to increase mortality rates
717 and canopy turnover in tropical forests (Phillips et al., 2010; Feldpausch et al., 2016; Leitold
718 et al., 2018); such disturbances may increase gap fraction and thus reduce gross primary
719 productivity and evapotranspiration in the years immediately following the drought. Fu-
720 ture studies that include dynamic vegetation can provide further insights on the resilience
721 and resistance of degraded and intact forests to climate extreme.

722 Our results show that structural changes resulting from forest degradation make
723 the forest surface drier and warmer (Figures 5-8 and S10). Drier and warmer conditions
724 near the surface increase flammability (Brando, Paolucci, et al., 2019, and references therein),
725 and it has been long suggested that forest degradation and canopy opening make forests
726 more likely to burn (e.g., Uhl & Buschbacher, 1985; Cochrane et al., 1999; Ray et al.,
727 2005; A. A. C. Alencar et al., 2015). The ED-2.2 simulations indeed predicted higher flamma-
728 bility in degraded (more open-canopy) forests on any given year (Figures 9 and S15). How-
729 ever, our results also suggest that climate strongly drives the variability of flammable
730 area across most of our study regions (Figures 9b and S15), which is consistent with the
731 significant increases in forest fires in the Amazon during extreme drought years (Morton
732 et al., 2013; Aragão et al., 2018). Moreover, our results indicate that differences in flammable
733 area between intact and degraded forests are reduced or even reversed during extreme
734 droughts, which indicates that under extreme conditions, the level of degradation is less
735 critical to create flammable conditions. This effect was predicted for most years at TAN,

736 which typically experiences severe and longer dry seasons compared to the other study
737 regions (Figure S15).

738 Previous studies suggest that parts of the Eastern Amazon could become drier by
739 the end of the century and experience more extreme events, including droughts (IPCC,
740 2014; Duffy et al., 2015), and thus potentially more susceptible to future fires (De Faria
741 et al., 2017; Brando et al., 2020). However, how tropical forest flammability will respond
742 in the long-term to ongoing changes in climate and land use is still uncertain, and re-
743 cent studies have shown that either climate (Le Page et al., 2017) or land use (Fonseca
744 et al., 2019) could be dominant on predicted shifts in fire regime. Importantly, while our
745 analysis focused on flammability, and ED-2.2 fire model captures the general patterns
746 of fire disturbance across the Amazon (Longo, Knox, Levine, et al., 2019), it does not
747 represent many mechanisms and processes that are critical to describe fire dynamics in
748 tropical forests, such as anthropogenic ignitions, diurnal cycle of fire intensity, and fire
749 termination, therefore we could not quantify the effects of fire on further forest degra-
750 dation. The use of process-based fire disturbance models within the ED-2.2 (e.g., Thon-
751 icke et al., 2010; Le Page et al., 2015) framework could contribute to further improve our
752 understanding of interactions between forest degradation, climate, and flammability across
753 the Amazon.

754 **5 Conclusion**

755 Our study showed that tropical forest degradation can markedly modify the ecosys-
756 tem functioning in the Amazon, with substantial reductions in evapotranspiration (ET)
757 and gross primary productivity (GPP), and increase in surface temperature (Figures 5-
758 8). Within the regions included in our study, the effects of degradation on energy, wa-
759 ter, and carbon cycles were the strongest in the Eastern and Southern Amazon, where
760 the dry season is more pronounced. Notably, in areas where severe forest degradation
761 resulted in substantial changes in forest structure, reductions in dry-season evapotran-
762 spiration are similar to those found in deforested areas (Figure 5; von Randow et al., 2004).
763 The area of the Amazon forest impacted by degradation is comparable to the deforested
764 area (Asner et al., 2005; Morton et al., 2013; Souza Jr. et al., 2013; Tyukavina et al., 2017),
765 and thus degradation-driven changes in water, energy, and carbon cycles are potentially
766 important. However, the extent to which degradation affects the biophysical and bio-
767 geochemical cycles at regional scale ultimately depends on (1) annual degradation rates;

768 (2) recovery time of degraded forests; and (3) the likelihood that degraded forests are
769 cleared. For example, (Brando, Silvério, et al., 2019) found that ET in burned forests
770 was indistinguishable from intact forests 7 years after the last fire. While their result sug-
771 gests fast recovery of degraded forests, the impacts of degradation on ET can still be re-
772 gionally relevant if degradation rates are sufficiently high to maintain low average age
773 since last disturbance in degraded forests. Moreover, we found that the impacts of trop-
774 ical forest degradation on energy, water, and carbon cycles and on flammability are more
775 pronounced during typical years than during extreme droughts (when all forests become
776 flammable), which highlights the complex interactions between climate and forest struc-
777 ture. To understand and reduce uncertainties of climate-structure interactions, it would
778 be valuable to leverage the recent advances in remote sensing of forest structure, includ-
779 ing the recently launched GEDI mission (Hancock et al., 2019), and terrestrial biosphere
780 models that can represent complex and heterogeneous ecosystems (Fisher et al., 2018).
781 Our study, while focusing on airborne lidar data, has demonstrated the opportunities
782 to integrate remote sensing and terrestrial biosphere models even in regions with com-
783 plex forest structure such as degraded forests.

784 **Acknowledgments**

785 Airborne lidar and forest inventory data were obtained from Sustainable Landscapes
786 Brazil (2019), dos-Santos et al. (2019) (Brazil) and Paracou Portal (2016) (French Guiana).
787 MERRA-2 reanalyses are available from GMAO (2015a, 2015b, 2015c, 2015d) and MSWEP-
788 2.2 data were downloaded from <http://www.gloh2o.org>. The ED-2.2 model used in this
789 study is available at Longo et al. (2019) and the scripts and ED-2.2 output are perma-
790 nently stored at Longo et al. (2020). Trait data are available at the TRY initiative on
791 plant traits (<http://www.try-db.org>), request 2751; at Gu et al. (2016); or as support-
792 ing information from the cited references (I. J. Wright et al., 2004; Santiago & Wright,
793 2007; Bahar et al., 2017).

794 The research was carried out at the Jet Propulsion Laboratory, California Insti-
795 tute of Technology, under a contract with the National Aeronautics and Space Admin-
796 istration (80NM0018D004), and supported by NASA Earth Sciences grant (NNH16ZDA001N-
797 IDS, grant 16-IDS16-0049). Data recorded at the Guyaflux tower were obtained thanks
798 to the support of two *Investissement d'avenir* grants from the Agence Nationale de la
799 Recherche (CEBA, ref ANR-10-LABX-25-01; ARBRE, ref. ANR-11-LABX-0002-01). Data

800 in Brazil were acquired by the Sustainable Landscapes Brazil project supported by the
 801 Brazilian Agricultural Research Corporation (EMBRAPA), the U.S. Forest Service, and
 802 USAID, and the U.S. Department of State. The study has been supported by the TRY
 803 initiative on plant traits, which is hosted, developed and maintained by J. Kattge and
 804 G. Bönisch (Max Planck Institute for Biogeochemistry, Jena, Germany). TRY is cur-
 805 rently supported by DIVERSITAS/Future Earth and the German Centre for Integra-
 806 tive Biodiversity Research (iDiv) Halle-Jena-Leipzig.

807 We thank Xiangtao Xu for sharing the trait plasticity algorithm and discussions
 808 on model results; Divino Silvério for processing and sharing the data from Tanguro; Hylke
 809 Beck for sharing the MSWEP-2.2 data; and Marcos Scaranello, Fabian Schneider, Alexan-
 810 dra Konings, and A. Anthony Bloom for discussions on the lidar initialization algorithm
 811 and interpretation of model results. The model simulations were carried out at the Odyssey
 812 cluster, supported by the FAS Division of Science, Research Computing Group at Har-
 813 vard University; and at the Brazilian National Laboratory for Scientific Computing (LNCC).
 814 M.L. was supported by the São Paulo State Research Foundation (FAPESP, 2015/07227-
 815 6) and by the NASA Postdoctoral Program, administered by Universities Space Research
 816 Association under contract with NASA. M.K. was supported in part by the Next Gen-
 817 eration Ecosystem Experiments-Tropics, funded by the U.S. Department of Energy, Of-
 818 fice of Science, Office of Biological and Environmental Research.

819 **References**

- 820 Achard, F., Beuchle, R., Mayaux, P., Stibig, H.-J., Bodart, C., Brink, A., . . . Simon-
 821 etti, D. (2014, Aug). Determination of tropical deforestation rates and related
 822 carbon losses from 1990 to 2010. *Glob. Change Biol.*, *20*(8), 2540–2554. doi:
 823 10.1111/gcb.12605
- 824 Alamgir, M., Campbell, M. J., Turton, S. M., Pert, P. L., Edwards, W., & Laurance,
 825 W. F. (2016, Jul). Degraded tropical rain forests possess valuable carbon stor-
 826 age opportunities in a complex, forested landscape. *Sci. Rep.*, *6*(30012). doi:
 827 10.1038/srep30012
- 828 Alencar, A., Nepstad, D., & Vera Diaz, M. C. (2006, Feb). Forest understory fire in
 829 the Brazilian Amazon in ENSO and non-ENSO years: Area burned and com-
 830 mitted carbon emissions. *Earth Interact.*, *10*(6), 1–17. doi: 10.1175/EI150.1
- 831 Alencar, A. A. C., Brando, P. M., Asner, G. P., & Putz, F. E. (2015, Sep). Land-

- 832 scape fragmentation, severe drought and the new Amazon forest fire regime.
833 *Ecol. Appl.*, *25*(6), 1493–1505. doi: 10.1890/14-1528.1
- 834 Antonarakis, A. S., Munger, J. W., & Moorcroft, P. R. (2014, Jul). Imaging
835 spectroscopy- and lidar-derived estimates of canopy composition and struc-
836 ture to improve predictions of forest carbon fluxes and ecosystem dynamics.
837 *Geophys. Res. Lett.*, *41*(7), 2535–2542. doi: 10.1002/2013GL058373
- 838 Antonarakis, A. S., Saatchi, S. S., Chazdon, R. L., & Moorcroft, P. R. (2011,
839 Jun). Using lidar and radar measurements to constrain predictions of for-
840 est ecosystem structure and function. *Ecol. Appl.*, *21*(4), 1120–1137. doi:
841 10.1890/10-0274.1
- 842 Aragão, L. E. O. C., Anderson, L. O., Fonseca, M. G., Rosan, T. M., Vedovato,
843 L. B., Wagner, F. H., ... Saatchi, S. (2018, Feb). 21st century drought-related
844 fires counteract the decline of Amazon deforestation carbon emissions. *Nature*
845 *Comm.*, *9*(1), 536. doi: 10.1038/s41467-017-02771-y
- 846 Aragão, L. E. O. C., Poulter, B., Barlow, J. B., Anderson, L. O., Malhi, Y., Saatchi,
847 S., ... Gloor, E. (2014, Nov). Environmental change and the carbon balance
848 of Amazonian forests. *Biol. Rev.*, *89*(4), 913–931. doi: 10.1111/brv.12088
- 849 Asner, G. P., Broadbent, E. N., Oliveira, P. J. C., Keller, M., Knapp, D. E., & Silva,
850 J. N. M. (2006, Aug). Condition and fate of logged forests in the Brazil-
851 ian Amazon. *Proc. Natl. Acad. Sci. U. S. A.*, *103*(34), 12947–12950. doi:
852 10.1073/pnas.0604093103
- 853 Asner, G. P., Knapp, D. E., Broadbent, E. N., Oliveira, P. J. C., Keller, M., &
854 Silva, J. N. (2005, Oct). Selective logging in the Brazilian Amazon. *Science*,
855 *310*(5747), 480–482. doi: 10.1126/science.1118051
- 856 Asner, G. P., Martin, R. E., Tupayachi, R., Anderson, C. B., Sinca, F., Carranza-
857 Jiménez, L., & Martinez, P. (2014, Apr). Amazonian functional diversity from
858 forest canopy chemical assembly. *Proc. Natl. Acad. Sci. U. S. A.*, *111*(15),
859 5604–5609. doi: 10.1073/pnas.1401181111
- 860 Asner, G. P., Powell, G. V. N., Mascaro, J., Knapp, D. E., Clark, J. K., Jacobson,
861 J., ... Hughes, R. F. (2010, Sep). High-resolution forest carbon stocks and
862 emissions in the Amazon. *Proc. Natl. Acad. Sci. U. S. A.*, *107*(38), 16738-
863 16742. doi: 10.1073/pnas.1004875107
- 864 Baccini, A., Walker, W., Carvalho, L., Farina, M., Sulla-Menashe, D., & Houghton,

- 865 R. A. (2017, Oct). Tropical forests are a net carbon source based on above-
866 ground measurements of gain and loss. *Science*, *358*(6360), 230–234. doi:
867 10.1126/science.aam5962
- 868 Bahar, N. H. A., Ishida, F. Y., Weerasinghe, L. K., Guerrieri, R., O’Sullivan, O. S.,
869 Bloomfield, K. J., ... Atkin, O. K. (2017, May). Leaf-level photosynthetic ca-
870 pacity in lowland Amazonian and high-elevation Andean tropical moist forests
871 of Peru. *New Phytol.*, *214*(3), 1002–1018. doi: 10.1111/nph.14079
- 872 Balch, J. K., Nepstad, D. C., Brando, P. M., Curran, L. M., Portela, O., de Car-
873 valho, O., & Lefebvre, P. (2008, Oct). Negative fire feedback in a transitional
874 forest of southeastern Amazonia. *Glob. Change Biol.*, *14*(10), 2276–2287. doi:
875 10.1111/j.1365-2486.2008.01655.x
- 876 Baraloto, C., Paine, C. E. T., Poorter, L., Beauchene, J., Bonal, D., Domen-
877 ach, A.-M., ... Chave, J. (2010, Nov). Decoupled leaf and stem eco-
878 nomics in rain forest trees. *Ecol. Lett.*, *13*(11), 1338–1347. doi: 10.1111/
879 j.1461-0248.2010.01517.x
- 880 Barkhordarian, A., von Storch, H., Behrangi, A., Loikith, P. C., Mechoso, C. R.,
881 & Detzer, J. (2018, Jun). Simultaneous regional detection of land-
882 use changes and elevated GHG levels: the case of spring precipitation in
883 tropical South America. *Geophys. Res. Lett.*, *45*(12), 6262–6271. doi:
884 10.1029/2018GL078041
- 885 Barlow, J., Lagan, B. O., & Peres, C. A. (2003, 5). Morphological correlates of
886 fire-induced tree mortality in a central Amazonian forest. *J. Trop. Ecol.*, *19*(3),
887 291–299. doi: 10.1017/S0266467403003328
- 888 Barlow, J., Lennox, G. D., Ferreira, J., Berenguer, E., Lees, A. C., Mac Nally, R.,
889 ... Gardner, T. A. (2016, Jul). Anthropogenic disturbance in tropical forests
890 can double biodiversity loss from deforestation. *Nature*, *535*, 144–147. doi:
891 10.1038/nature18326
- 892 Beck, H. E., Wood, E. F., Pan, M., Fisher, C. K., Miralles, D. G., van Dijk, A. I.,
893 ... Adler, R. F. (2019, Mar). MSWEP V2 global 3-hourly 0.1° precipitation:
894 methodology and quantitative assessment. *Bull. Am. Meteorol. Soc.*, *100*(3),
895 473–500. doi: 10.1175/BAMS-D-17-0138.1
- 896 Berenguer, E., Ferreira, J., Gardner, T. A., Aragão, L. E. O. C., de Camargo, P. B.,
897 Cerri, C. E., ... Barlow, J. (2014, Dec). A large-scale field assessment of

- 898 carbon stocks in human-modified tropical forests. *Glob. Change Biol.*, 20(12),
899 3713–3726. doi: 10.1111/gcb.12627
- 900 Blair, J. B., & Hofton, M. A. (1999, Aug). Modeling laser altimeter return wave-
901 forms over complex vegetation using high-resolution elevation data. *Geophys.*
902 *Res. Lett.*, 26(16), 2509–2512. doi: 10.1029/1999GL010484
- 903 Blanc, L., Echard, M., Herault, B., Bonal, D., Marcon, E., Chave, J., & Baraloto, C.
904 (2009, Sep). Dynamics of aboveground carbon stocks in a selectively logged
905 tropical forest. *Ecol. Appl.*, 19(6), 1397–1404. doi: 10.1890/08-1572.1
- 906 Bogan, S. A., Antonarakis, A. S., & Moorcroft, P. R. (2019, Jul). Imag-
907 ing spectrometry-derived estimates of regional ecosystem composition for
908 the Sierra Nevada, California. *Remote Sens. Environ.*, 228, 14–30. doi:
909 10.1016/j.rse.2019.03.031
- 910 Bonal, D., Bosc, A., Ponton, S., Goret, J.-Y., Burban, B., Gross, P., ... Granier,
911 A. (2008, Aug). Impact of severe dry season on net ecosystem exchange
912 in the Neotropical rainforest of French Guiana. *Glob. Change Biol.*, 14(8),
913 1917–1933. doi: 10.1111/j.1365-2486.2008.01610.x
- 914 Both, S., Riutta, T., Paine, C. E. T., Elias, D. M. O., Cruz, R. S., Jain, A., ...
915 Burslem, D. F. R. P. (2019, Feb). Logging and soil nutrients independently ex-
916 plain plant trait expression in tropical forests. *New Phytol.*, 221(4), 1853–1865.
917 doi: 10.1111/nph.15444
- 918 Braghieri, R. K., Quaife, T., Black, E., He, L., & Chen, J. M. (2019, Nov). Underes-
919 timation of global photosynthesis in earth system models due to representation
920 of vegetation structure. *Global Biogeochem. Cycles*, 33(11), 1358–1369. doi:
921 10.1029/2018GB006135
- 922 Brando, P. M., Balch, J. K., Nepstad, D. C., Morton, D. C., Putz, F. E., Coe,
923 M. T., ... Soares-Filho, B. S. (2014, Apr). Abrupt increases in Amazonian
924 tree mortality due to drought–fire interactions. *Proc. Natl. Acad. Sci. U. S. A.*,
925 111(17), 6347–6352. doi: 10.1073/pnas.1305499111
- 926 Brando, P. M., Nepstad, D. C., Balch, J. K., Bolker, B., Christman, M. C., Coe, M.,
927 & Putz, F. E. (2012, Feb). Fire-induced tree mortality in a neotropical forest:
928 the roles of bark traits, tree size, wood density and fire behavior. *Glob. Change*
929 *Biol.*, 18(2), 630–641. doi: 10.1111/j.1365-2486.2011.02533.x
- 930 Brando, P. M., Paolucci, L., Ummenhofer, C. C., Ordway, E. M., Hartmann, H.,

- 931 Cattau, M. E., ... Balch, J. (2019, May). Droughts, wildfires, and forest
 932 carbon cycling: A pantropical synthesis. *Annu. Rev. Earth Pl. Sc.*, *47*(1),
 933 555–581. doi: 10.1146/annurev-earth-082517-010235
- 934 Brando, P. M., Silvério, D., Maracahipes-Santos, L., Oliveira-Santos, C., Levick,
 935 S. R., Coe, M. T., ... Trumbore, S. E. (2019, Sep). Prolonged tropical forest
 936 degradation due to compounding disturbances: implications for CO₂ and H₂O
 937 fluxes of an experimental forest. *Glob. Change Biol.*, *25*(9), 2855–2868. doi:
 938 10.1111/gcb.14659
- 939 Brando, P. M., Soares Filho, B., Rodrigues, L., Assunção, A., Morton, D., Tuch-
 940 schneider, D., ... Coe, M. T. (2020, Jan). The gathering firestorm in southern
 941 Amazonia. *Sci. Adv.*, *6*(2), eaay1632. doi: 10.1126/sciadv.aay1632
- 942 Brum, M., Vadeboncoeur, M. A., Ivanov, V., Asbjornsen, H., Saleska, S., Alves,
 943 L. F., ... Oliveira, R. S. (2019, Jan). Hydrological niche segregation defines
 944 forest structure and drought tolerance strategies in a seasonal Amazon forest.
 945 *J. Ecol.*, *107*(1), 318–333. doi: 10.1111/1365-2745.13022
- 946 Bustamante, M. M. C., Roitman, I., Aide, T. M., Alencar, A., Anderson, L., Aragão,
 947 L., ... Vieira, I. C. (2016, Jan). Towards an integrated monitoring frame-
 948 work to assess the effects of tropical forest degradation and recovery on
 949 carbon stocks and biodiversity. *Glob. Change Biol.*, *22*(1), 92–109. doi:
 950 10.1111/gcb.13087
- 951 Calders, K., Newnham, G., Burt, A., Murphy, S., Raumonon, P., Herold, M., ...
 952 Kaasalainen, M. (2015, Feb). Nondestructive estimates of above-ground
 953 biomass using terrestrial laser scanning. *Methods Ecol. Evol.*, *6*(2), 198–208.
 954 doi: 10.1111/2041-210X.12301
- 955 Chave, J., Condit, R., Aguilar, S., Hernandez, A., Lao, S., & Perez, R. (2004, Mar).
 956 Error propagation and scaling for tropical forest biomass estimates. *Philos.*
 957 *Trans. R. Soc. B-Biol. Sci.*, *359*(1443), 409–420. doi: 10.1098/rstb.2003.1425
- 958 Chave, J., Coomes, D., Jansen, S., Lewis, S. L., Swenson, N. G., & Zanne, A. E.
 959 (2009, Apr). Towards a worldwide wood economics spectrum. *Ecol. Lett.*,
 960 *12*(4), 351–366. doi: 10.1111/j.1461-0248.2009.01285.x
- 961 Chave, J., Réjou-Méchain, M., Búrquez, A., Chidumayo, E., Colgan, M. S., Delitti,
 962 W. B., ... Vieilledent, G. (2014, Oct). Improved allometric models to esti-
 963 mate the aboveground biomass of tropical trees. *Glob. Change Biol.*, *20*(10),

- 964 3177–3190. doi: 10.1111/gcb.12629
- 965 Cochran, M. A., Alencar, A., Schulze, M. D., Souza, C. M., Nepstad, D. C., Lefeb-
966 vre, P., & Davidson, E. A. (1999, Jun). Positive feedbacks in the fire dy-
967 namic of closed canopy tropical forests. *Science*, *284*(5421), 1832–1835. doi:
968 10.1126/science.284.5421.1832
- 969 Davidson, E. A., de Araújo, A. C., Artaxo, P., Balch, J. K., Brown, I. F., Bus-
970 tamante, M. M. C., ... Wofsy, S. C. (2012, Jan). The Amazon basin in
971 transition. *Nature*, *481*(7381), 321–328. doi: 10.1038/nature10717
- 972 de Almeida, C. T., Galvão, L. S., Aragão, L. E. d. O. C. e., Ometto, J. P. H. B., Ja-
973 con, A. D., Pereira, F. R. d. S., ... Longo, M. (2019, Oct). Combining LiDAR
974 and hyperspectral data for aboveground biomass modeling in the Brazilian
975 Amazon using different regression algorithms. *Remote Sens. Environ.*, *232*,
976 111323. doi: 10.1016/j.rse.2019.111323
- 977 De Faria, B. L., Brando, P. M., Macedo, M. N., Panday, P. K., Soares Filho, B. S.,
978 & Coe, M. T. (2017, Sep). Current and future patterns of fire-induced
979 forest degradation in Amazonia. *Environ. Res. Lett.*, *12*(9), 095005. doi:
980 10.1088/1748-9326/aa69ce
- 981 de Resende, A. F., Nelson, B. W., Flores, B. M., & de Almeida, D. R. (2014, Nov).
982 Fire damage in seasonally flooded and upland forests of the Central Amazon.
983 *Biotropica*, *46*(6), 643–646. doi: 10.1111/btp.12153
- 984 d’Oliveira, M. V. N., Reutebuch, S. E., McGaughey, R. J., & Andersen, H.-E.
985 (2012, Sep). Estimating forest biomass and identifying low-intensity log-
986 ging areas using airborne scanning lidar in Antimary State Forest, Acre
987 state, western Brazilian Amazon. *Remote Sens. Environ.*, *124*, 479–491.
988 doi: 10.1016/j.rse.2012.05.014
- 989 dos-Santos, M., Keller, M., & Morton, D. (2019, Dec). *LiDAR surveys over se-*
990 *lected forest research sites, Brazilian Amazon, 2008–2018*. Retrieved 31 Jan
991 2020, from https://daac.ornl.gov/cgi-bin/dsviewer.pl?ds_id=1644 doi:
992 10.3334/ORNLDAAC/1644
- 993 Duffy, P. B., Brando, P., Asner, G. P., & Field, C. B. (2015, Oct). Projections of fu-
994 ture meteorological drought and wet periods in the Amazon. *Proc. Natl. Acad.*
995 *Sci. U. S. A.*, *112*(43), 13172–13177. doi: 10.1073/pnas.1421010112
- 996 Erb, K.-H., Fetzl, T., Plutzer, C., Kastner, T., Lauk, C., Mayer, A., ... Haberl, H.

- 997 (2016, Sep). Biomass turnover time in terrestrial ecosystems halved by land
 998 use. *Nature Geosci.*, *9*(9), 674–678. doi: 10.1038/ngeo2782
- 999 Erb, K.-H., Kastner, T., Plutzer, C., Bais, A. L. S., Carvalhais, N., Fetzel, T., ...
 1000 Luysaert, S. (2018, Jan). Unexpectedly large impact of forest management
 1001 and grazing on global vegetation biomass. *Nature*, *553*(7686), 73–76. doi:
 1002 10.1038/nature25138
- 1003 Falster, D. S., Duursma, R. A., Ishihara, M. I., Barneche, D. R., FitzJohn, R. G.,
 1004 Vårhammar, A., ... York, R. A. (2015, May). BAAD: a biomass and
 1005 allometry database for woody plants. *Ecology*, *96*(5), 1445–1445. doi:
 1006 10.1890/14-1889.1
- 1007 Falster, D. S., FitzJohn, R. G., Brännström, Å., Dieckmann, U., & Westoby, M.
 1008 (2016, Feb). **plant**: A package for modelling forest trait ecology and evolution.
 1009 *Methods Ecol. Evol.*, *7*(2), 136–146. doi: 10.1111/2041-210X.12525
- 1010 Fan, Y., Miguez-Macho, G., Jobbágy, E. G., Jackson, R. B., & Otero-Casal, C.
 1011 (2017, Oct). Hydrologic regulation of plant rooting depth. *Proc. Natl. Acad.*
 1012 *Sci. U. S. A.*, *114*(40), 10572–10577. doi: 10.1073/pnas.1712381114
- 1013 Feldpausch, T. R., Banin, L., Phillips, O. L., Baker, T. R., Lewis, S. L., Quesada,
 1014 C. A., ... Lloyd, J. (2011, May). Height-diameter allometry of tropical forest
 1015 trees. *Biogeosciences*, *8*(5), 1081–1106. doi: 10.5194/bg-8-1081-2011
- 1016 Feldpausch, T. R., Jirka, S., Passos, C. A. M., Jasper, F., & Riha, S. J. (2005,
 1017 11). When big trees fall: Damage and carbon export by reduced impact log-
 1018 ging in southern Amazonia. *Forest Ecol. Manag.*, *219*(2–3), 199–215. doi:
 1019 10.1016/j.foreco.2005.09.003
- 1020 Feldpausch, T. R., Lloyd, J., Lewis, S. L., Brienien, R. J. W., Gloor, M., Mon-
 1021 teagudo Mendoza, A., ... Phillips, O. L. (2012, Aug). Tree height integrated
 1022 into pantropical forest biomass estimates. *Biogeosciences*, *9*(8), 3381–3403.
 1023 doi: 10.5194/bg-9-3381-2012
- 1024 Feldpausch, T. R., Phillips, O. L., Brienien, R. J. W., Gloor, E., Lloyd, J., Lopez-
 1025 Gonzalez, G., ... Vos, V. A. (2016, Jul). Amazon forest response to
 1026 repeated droughts. *Global Biogeochem. Cycles*, *30*(7), 964–982. doi:
 1027 10.1002/2015GB005133
- 1028 Ferraz, A., Saatchi, S., Longo, M., & Clark, D. B. (2020). Tropical tree size demog-
 1029 raphy from airborne lidar. *Ecol. Appl.*. (advance online publication) doi: 10

- 1030 .1002/eap.2154
- 1031 Ferraz, A., Saatchi, S., Mallet, C., & Meyer, V. (2016, Sep). Lidar detection of indi-
 1032 vidual tree size in tropical forests. *Remote Sens. Environ.*, *183*, 318–333. doi:
 1033 10.1016/j.rse.2016.05.028
- 1034 Ferraz, A., Saatchi, S., Xu, L., Hagen, S., Chave, J., Yu, Y., ... Ganguly, S. (2018,
 1035 Sep). Carbon storage potential in degraded forests of Kalimantan, Indonesia.
 1036 *Environ. Res. Lett.*, *13*(9), 095001. doi: 10.1088/1748-9326/aad782
- 1037 Fischer, F. J., Maréchaux, I., & Chave, J. (2019). Improving plant allometry by fus-
 1038 ing forest models and remote sensing. *New Phytol.* (advance online publica-
 1039 tion) doi: 10.1111/nph.15810
- 1040 Fischer, R., Bohn, F., de Paula, M. D., Dislich, C., Groeneveld, J., Gutiérrez, A. G.,
 1041 ... Huth, A. (2016, Apr). Lessons learned from applying a forest gap model to
 1042 understand ecosystem and carbon dynamics of complex tropical forests. *Ecol.*
 1043 *Model.*, *326*, 124–133. doi: 10.1016/j.ecolmodel.2015.11.018
- 1044 Fisher, R. A., Koven, C. D., Anderegg, W. R. L., Christoffersen, B. O., Dietze,
 1045 M. C., Farrior, C., ... Moorcroft, P. (2018, Jan). Vegetation demographics in
 1046 Earth system models: a review of progress and priorities. *Glob. Change Biol.*,
 1047 *24*(1), 35–54. doi: 10.1111/gcb.13910
- 1048 Fonseca, M. G., Alves, L. M., Aguiar, A. P. D., Arai, E., Anderson, L. O., Rosan,
 1049 T. M., ... de Aragão, L. E. O. e. C. (2019). Effects of climate and land-use
 1050 change scenarios on fire probability during the 21st century in the Brazilian
 1051 Amazon. *Glob. Change Biol.* doi: 10.1111/gcb.14709
- 1052 Friedlingstein, P., Jones, M. W., O’Sullivan, M., Andrew, R. M., Hauck, J., Peters,
 1053 G. P., ... Zaehle, S. (2019, Dec). Global carbon budget 2019. *Earth Syst. Sci.*
 1054 *Data*, *11*(4), 1783–1838. doi: 10.5194/essd-11-1783-2019
- 1055 Fu, R., Yin, L., Li, W., Arias, P. A., Dickinson, R. E., Huang, L., ... Myneni, R. B.
 1056 (2013, Nov). Increased dry-season length over southern Amazonia in recent
 1057 decades and its implication for future climate projection. *Proc. Natl. Acad.*
 1058 *Sci. U. S. A.*, *110*(45), 18110–18115. doi: 10.1073/pnas.1302584110
- 1059 Gelaro, R., McCarty, W., Suárez, M. J., Todling, R., Molod, A., Takacs, L., ...
 1060 Zhao, B. (2017, Jul). The Modern-Era Retrospective analysis for Research
 1061 and Applications, version 2 (MERRA-2). *J. Climate*, *30*(14), 5419–5454. doi:
 1062 10.1175/JCLI-D-16-0758.1

- 1063 Ghazoul, J., & Chazdon, R. (2017, Oct). Degradation and recovery in changing for-
 1064 est landscapes: A multiscale conceptual framework. *Ann. Rev. Environ. Res.*,
 1065 42(1), 161–188. doi: 10.1146/annurev-environ-102016-060736
- 1066 GMAO. (2015a). *MERRA-2 tavg1_2d_flux_Nx: 2d, 1-hourly, time-averaged,*
 1067 *single-level, assimilation, surface flux diagnostics V5.12.4.* Retrieved 06
 1068 Sep 2018, from <https://doi.org/10.5067/7MCPBJ41Y0K6> doi: 10.5067/
 1069 7MCPBJ41Y0K6
- 1070 GMAO. (2015b). *MERRA-2 tavg1_2d_lnd_Nx: 2d, 1-hourly, time-averaged,*
 1071 *single-level, assimilation, land surface diagnostics V5.12.4.* Retrieved
 1072 06 Sep 2018, from <https://doi.org/10.5067/RKPHT8KC1Y1T> doi:
 1073 10.5067/RKPHT8KC1Y1T
- 1074 GMAO. (2015c). *MERRA-2 tavg1_2d_rad_Nx: 2d, 1-hourly, time-averaged, single-*
 1075 *level, assimilation, radiation diagnostics V5.12.4.* Retrieved 06 Sep 2018, from
 1076 <https://doi.org/10.5067/Q9QMY5PBNV1T> doi: 10.5067/Q9QMY5PBNV1T
- 1077 GMAO. (2015d). *MERRA-2 tavg1_2d_slv_Nx: 2d, 1-hourly, time-averaged,*
 1078 *single-level, assimilation, single-level diagnostics V5.12.4.* Retrieved 06
 1079 Sep 2018, from <https://doi.org/10.5067/VJAFPLI1CSIV> doi: 10.5067/
 1080 VJAFPLI1CSIV
- 1081 Gourlet-Fleury, S., Ferry, B., Molino, J.-F., Petronelli, P., & Schmitt, L. (2004).
 1082 Experimental plots: Key features. In S. Gourlet-Fleury, J.-M. Guehl, &
 1083 O. Laroussinie (Eds.), *Ecology and management of a Neotropical rainforest:*
 1084 *Lessons drawn from Paracou, a long-term experimental research site in French*
 1085 *Guiana* (pp. 3–60). Paris: Elsevier.
- 1086 Gourlet-Fleury, S., Guehl, J.-M., & Laroussinie, O. (2004). *Ecology and manage-*
 1087 *ment of a Neotropical rainforest: Lessons drawn from Paracou, a long-term*
 1088 *experimental research site in French Guiana*. Paris: Elsevier.
- 1089 Grace, J., Mitchard, E., & Gloor, E. (2014, Oct). Perturbations in the carbon bud-
 1090 get of the tropics. *Glob. Change Biol.*, 20(10), 3238–3255. doi: 10.1111/gcb
 1091 .12600
- 1092 Grossiord, C., Buckley, T. N., Cernusak, L. A., Novick, K. A., Poulter, B., Siegwolf,
 1093 R. T. W., . . . McDowell, N. G. (2020, Jun). Plant responses to rising vapor
 1094 pressure deficit. *New Phytol.*, 226(6), 1550–1566. doi: 10.1111/nph.16485
- 1095 Gu, L., Norby, R., Haworth, I., Jensen, A., Turner, B., Walker, A., . . . Winter, K.

- 1096 (2016). *Photosynthetic parameters and nutrient content of trees at the Panama*
 1097 *crane sites. 1.0. NGEE Tropics data collection.* Retrieved 12 Sep 2019, from
 1098 <https://ngt-data.lbl.gov> doi: 10.15486/NGT/1255260
- 1099 Haddad, N. M., Brudvig, L. A., Clobert, J., Davies, K. F., Gonzalez, A., Holt,
 1100 R. D., ... Townshend, J. R. (2015, Mar). Habitat fragmentation and its
 1101 lasting impact on Earth's ecosystems. *Science Advances*, *1*(2), e1500052. doi:
 1102 10.1126/sciadv.1500052
- 1103 Hancock, S., Armston, J., Hofton, M., Sun, X., Tang, H., Duncanson, L. I., ...
 1104 Dubayah, R. (2019, Feb). The GEDI simulator: A large-footprint waveform
 1105 lidar simulator for calibration and validation of spaceborne missions. *Earth*
 1106 *Space Sci.*, *6*(2), 290–310. doi: 10.1029/2018EA000506
- 1107 Hansen, M. C., Potapov, P. V., Moore, R., Hancher, M., Turubanova, S. A.,
 1108 Tyukavina, A., ... Townshend, J. R. G. (2013, Nov). High-resolution global
 1109 maps of 21st-century forest cover change. *Science*, *342*(6160), 850–853. doi:
 1110 10.1126/science.1244693
- 1111 Harris, N. L., Brown, S., Hagen, S. C., Saatchi, S. S., Petrova, S., Salas, W., ...
 1112 Lotsch, A. (2012, Jun). Baseline map of carbon emissions from deforestation in
 1113 tropical regions. *Science*, *336*(6088), 1573–1576. doi: 10.1126/science.1217962
- 1114 Hayek, M. N., Longo, M., Wu, J., Smith, M. N., Restrepo-Coupe, N., Tapajós,
 1115 R., ... Wofsy, S. C. (2018, Aug). Carbon exchange in an Amazon
 1116 forest: from hours to years. *Biogeosciences*, *15*(15), 4833–4848. doi:
 1117 10.5194/bg-15-4833-2018
- 1118 Hérault, B., & Piponiot, C. (2018, Feb). Key drivers of ecosystem recovery after dis-
 1119 turbance in a neotropical forest. *Forest Ecosyst.*, *5*(1), 2. doi: 10.1186/s40663
 1120 -017-0126-7
- 1121 Hess, L. L., Melack, J. M., Affonso, A. G., Barbosa, C., Gastil-Buhl, M., & Novo,
 1122 E. M. L. M. (2015, Aug). Wetlands of the lowland Amazon Basin: Ex-
 1123 tent, vegetative cover, and dual-season inundated area as mapped with
 1124 JERS-1 synthetic aperture radar. *Wetlands*, *35*(4), 745–756. doi: 10.1007/
 1125 s13157-015-0666-y
- 1126 Hirano, T., Kusin, K., Limin, S., & Osaki, M. (2015, May). Evapotranspiration of
 1127 tropical peat swamp forests. *Glob. Change Biol.*, *21*(5), 1914–1927. doi: 10
 1128 .1111/gcb.12653

- 1129 Holdaway, R. J., Sparrow, A. D., & Coomes, D. A. (2010, May). Trends in entropy
 1130 production during ecosystem development in the Amazon Basin. *Philos. Trans.*
 1131 *R. Soc. B-Biol. Sci.*, *365*(1545), 1437–1447. doi: 10.1098/rstb.2009.0298
- 1132 Hosonuma, N., Herold, M., De Sy, V., De Fries, R. S., Brockhaus, M., Verchot, L.,
 1133 ... Romijn, E. (2012, Apr). An assessment of deforestation and forest degra-
 1134 dation drivers in developing countries. *Environ. Res. Lett.*, *7*(4), 044009. doi:
 1135 10.1088/1748-9326/7/4/044009
- 1136 Huang, M., & Asner, G. P. (2010, Sep). Long-term carbon loss and recovery fol-
 1137 lowing selective logging in Amazon forests. *Global Biogeochem. Cycles*, *24*(3),
 1138 GB3028. doi: 10.1029/2009GB003727
- 1139 Huang, M., Asner, G. P., Keller, M., & Berry, J. A. (2008, Mar). An ecosystem
 1140 model for tropical forest disturbance and selective logging. *J. Geophys. Res.-*
 1141 *Biogeosci.*, *113*(G1), G01002. doi: 10.1029/2007JG000438
- 1142 Hunter, M. O., Keller, M., Vitoria, D., & Morton, D. C. (2013, Dec). Tree height
 1143 and tropical forest biomass estimation. *Biogeosciences*, *10*(6), 10491–10529.
 1144 doi: 10.5194/bg-10-8385-2013
- 1145 Hurtt, G. C., Dubayah, R., Drake, J., Moorcroft, P. R., Pacala, S. W., Blair, J. B.,
 1146 & Fearon, M. G. (2004, Jun). Beyond potential vegetation: combining lidar
 1147 data and a height-structured model for carbon studies. *Ecol. Appl.*, *14*(3),
 1148 873–883. doi: 10.1890/02-5317
- 1149 INMET. (2019, May). *Normais climatológicas do Brasil: 1981-2010*. Retrieved 15
 1150 May 2019, from [http://www.inmet.gov.br/portal/index.php?r=clima/
 1151 normaisClimatologicas](http://www.inmet.gov.br/portal/index.php?r=clima/normaisClimatologicas) (In Portuguese)
- 1152 IPCC. (2014). *Climate change 2014: impacts, adaptation, and vulnerability. part b:
 1153 regional aspects. contribution of working group ii to the fifth assessment report
 1154 of the Intergovernmental Panel on Climate Change* (V. R. Barros et al., Eds.).
 1155 Cambridge, UK and New York, NY, USA: Cambridge Univ. Press.
- 1156 Jucker, T., Caspersen, J., Chave, J., Antin, C., Barbier, N., Bongers, F., ...
 1157 Coomes, D. A. (2017, Jan). Allometric equations for integrating remote
 1158 sensing imagery into forest monitoring programmes. *Glob. Change Biol.*, *23*(1),
 1159 177–190. doi: 10.1111/gcb.13388
- 1160 Jucker, T., Hardwick, S. R., Both, S., Elias, D. M., Ewers, R. M., Milodowski, D. T.,
 1161 ... Coomes, D. A. (2018, Nov). Canopy structure and topography jointly con-

- 1162 strain the microclimate of human-modified tropical landscapes. *Glob. Change*
 1163 *Biol.*, *24*(11), 5243–5258. doi: 10.1111/gcb.14415
- 1164 Kapos, V. (1989, May). Effects of isolation on the water status of forest
 1165 patches in the brazilian amazon. *J. Trop. Ecol.*, *5*(2), 173–185. doi:
 1166 10.1017/S0266467400003448
- 1167 Kattge, J., Bönisch, G., Díaz, S., Lavorel, S., Prentice, I. C., Leadley, P., ... Wirth,
 1168 C. (2020, Jan). TRY plant trait database — enhanced coverage and open
 1169 access. *Glob. Change Biol.*, *26*(1), 119–188. doi: 10.1111/gcb.14904
- 1170 Kattge, J., Díaz, S., Lavorel, S., Prentice, I. C., Leadley, P., Bönisch, G., ... Wirth,
 1171 C. (2011, Sep). TRY – a global database of plant traits. *Glob. Change Biol.*,
 1172 *17*(9), 2905–2935. doi: 10.1111/j.1365-2486.2011.02451.x
- 1173 Kattge, J., Knorr, W., Raddatz, T., & Wirth, C. (2009, Apr). Quantifying pho-
 1174 tosynthetic capacity and its relationship to leaf nitrogen content for global-
 1175 scale terrestrial biosphere models. *Glob. Change Biol.*, *15*(4), 976–991. doi:
 1176 10.1111/j.1365-2486.2008.01744.x
- 1177 Keenan, T. F., & Niinemets, Ü. (2016, Dec). Global leaf trait estimates biased due
 1178 to plasticity in the shade. *Nat. Plants*, *3*, 16201. doi: 10.1038/nplants.2016
 1179 .201
- 1180 Knox, R. G., Longo, M., Swann, A. L. S., Zhang, K., Levine, N. M., Moorcroft,
 1181 P. R., & Bras, R. L. (2015, Jan). Hydrometeorological effects of historical
 1182 land-conversion in an ecosystem-atmosphere model of Northern South Amer-
 1183 ica. *Hydrol. Earth Syst. Sci.*, *19*(1), 241–273. doi: 10.5194/hess-19-241-2015
- 1184 Koven, C. D., Knox, R. G., Fisher, R. A., Chambers, J., Christoffersen, B. O.,
 1185 Davies, S. J., ... Xu, C. (2019). Benchmarking and parameter sensitivity
 1186 of physiological and vegetation dynamics using the functionally assembled
 1187 terrestrial ecosystem simulator (FATES) at Barro Colorado Island, Panama.
 1188 *Biogeosciences Discuss.*, *2019*, 1–46. (in press) doi: 10.5194/bg-2019-409
- 1189 Laybros, A., Schläpfer, D., Féret, J.-B., Descroix, L., Bedeau, C., Lefevre, M.-J., &
 1190 Vincent, G. (2019, Apr). Across date species detection using airborne imaging
 1191 spectroscopy. *Remote Sens.*, *11*(7), 789. doi: 10.3390/rs11070789
- 1192 Lees, J. M. (2017). RSEIS: Seismic time series analysis tools [Computer software
 1193 manual]. Retrieved from <https://CRAN.R-project.org/package=RSEIS> (R
 1194 package version 3.7-4)

- 1195 Lei, Y., Treuhaft, R., Keller, M., dos-Santos, M., Gonçalves, F., & Neumann,
 1196 M. (2018, Jun). Quantification of selective logging in tropical forest with
 1197 spaceborne SAR interferometry. *Remote Sens. Environ.*, *211*, 167–183. doi:
 1198 10.1016/j.rse.2018.04.009
- 1199 Leitold, V., Keller, M., Morton, D., Cook, B., & Shimabukuro, Y. (2015, Feb).
 1200 Airborne lidar-based estimates of tropical forest structure in complex terrain:
 1201 opportunities and trade-offs for REDD+. *Carbon Balance Manage.*, *10*(1), 3.
 1202 doi: 10.1186/s13021-015-0013-x
- 1203 Leitold, V., Morton, D. C., Longo, M., dos-Santos, M. N., Keller, M., & Scaranello,
 1204 M. (2018, Aug). El Niño drought increased canopy turnover in Amazon forests.
 1205 *New Phytol.*, *219*(3), 959–971. doi: 10.1111/nph.15110
- 1206 Le Page, Y., Morton, D., Bond-Lamberty, B., Pereira, J. M. C., & Hurtt, G. (2015,
 1207 Feb). HESFIRE: a global fire model to explore the role of anthropogenic and
 1208 weather drivers. *Biogeosciences*, *12*(3), 887–903. doi: 10.5194/bg-12-887-2015
- 1209 Le Page, Y., Morton, D., Hartin, C., Bond-Lamberty, B., Pereira, J. M. C., Hurtt,
 1210 G., & Asrar, G. (2017, Dec). Synergy between land use and climate change
 1211 increases future fire risk in Amazon forests. *Earth Syst. Dynam.*, *8*(4), 1237–
 1212 1246. doi: 10.5194/esd-8-1237-2017
- 1213 Levine, N. M., Zhang, K., Longo, M., Baccini, A., Phillips, O. L., Lewis, S. L., ...
 1214 Moorcroft, P. R. (2016, Jan). Ecosystem heterogeneity determines the re-
 1215 siliance of the Amazon to climate change. *Proc. Natl. Acad. Sci. U. S. A.*,
 1216 *113*(3), 793–797. doi: 10.1073/pnas.1511344112
- 1217 Lewis, S. L., Edwards, D. P., & Galbraith, D. (2015, Aug). Increasing human dom-
 1218 inance of tropical forests. *Science*, *349*(6250), 827–832. doi: 10.1126/science
 1219 .aaa9932
- 1220 Lloyd, J., Patiño, S., Paiva, R. Q., Nardoto, G. B., Quesada, C. A., Santos, A. J. B.,
 1221 ... Mercado, L. M. (2010, Jun). Optimisation of photosynthetic carbon gain
 1222 and within-canopy gradients of associated foliar traits for Amazon forest trees.
 1223 *Biogeosciences*, *7*(6), 1833–1859. doi: 10.5194/bg-7-1833-2010
- 1224 Lombardozzi, D. L., Smith, N. G., Cheng, S. J., Dukes, J. S., Sharkey, T. D.,
 1225 Rogers, A., ... Bonan, G. B. (2018, Jul). Triose phosphate limitation in
 1226 photosynthesis models reduces leaf photosynthesis and global terrestrial carbon
 1227 storage. *Environ. Res. Lett.*, *13*(7), 074025. doi: 10.1088/1748-9326/aacf68

- 1228 Longo, M., Keller, M., dos-Santos, M. N., Morton, D., Moorcroft, P. R., Vincent, G.,
 1229 ... Saatchi, S. (2020, Feb). Supporting dataset for “Impacts of degradation
 1230 on water, energy, and carbon cycling of the Amazon tropical forests”. *Zenodo*.
 1231 doi: 10.5281/zenodo.3634131
- 1232 Longo, M., Keller, M., dos Santos, M. N., Leitold, V., Pinagé, E. R., Baccini, A., ...
 1233 Morton, D. C. (2016, Nov). Aboveground biomass variability across intact and
 1234 degraded forests in the Brazilian Amazon. *Global Biogeochem. Cycles*, *30*(11),
 1235 1639–1660. doi: 10.1002/2016GB005465
- 1236 Longo, M., Knox, R., Medvigy, D. M., Levine, N. M., Dietze, M., Swann, A. L. S.,
 1237 ... Moorcroft, P. (2019, Aug). Ecosystem Demography model, version 2.2
 1238 (ed-2.2). *Zenodo*. doi: 10.5281/zenodo.3365659
- 1239 Longo, M., Knox, R. G., Levine, N. M., Alves, L. F., Bonal, D., Camargo, P. B., ...
 1240 Moorcroft, P. R. (2018, Aug). Ecosystem heterogeneity and diversity mitigate
 1241 Amazon forest resilience to frequent extreme droughts. *New Phytol.*, *219*(3),
 1242 914–931. doi: 10.1111/nph.15185
- 1243 Longo, M., Knox, R. G., Levine, N. M., Swann, A. L. S., Medvigy, D. M., Dietze,
 1244 M. C., ... Moorcroft, P. R. (2019, Oct). The biophysics, ecology, and bio-
 1245 geochemistry of functionally diverse, vertically and horizontally heterogeneous
 1246 ecosystems: the Ecosystem Demography model, version 2.2 – part 2: Model
 1247 evaluation for tropical South America. *Geosci. Model Dev.*, *12*(10), 4347–4374.
 1248 doi: 10.5194/gmd-12-4347-2019
- 1249 Longo, M., Knox, R. G., Medvigy, D. M., Levine, N. M., Dietze, M. C., Kim, Y., ...
 1250 Moorcroft, P. R. (2019, Oct). The biophysics, ecology, and biogeochemistry
 1251 of functionally diverse, vertically and horizontally heterogeneous ecosystems:
 1252 the Ecosystem Demography model, version 2.2 – part 1: Model description.
 1253 *Geosci. Model Dev.*, *12*(10), 4309–4346. doi: 10.5194/gmd-12-4309-2019
- 1254 MacArthur, R. H., & Horn, H. S. (1969, Sep). Foliage profile by vertical measure-
 1255 ments. *Ecology*, *50*(5), 802–804. doi: 10.2307/1933693
- 1256 Maréchaux, I., & Chave, J. (2017, Nov). An individual-based forest model to jointly
 1257 simulate carbon and tree diversity in Amazonia: description and applications.
 1258 *Ecol. Monogr.*, *87*(4), 632–664. doi: 10.1002/ecm.1271
- 1259 Martins, F. S. R. V., Xaud, H. A. M., dos Santos, J. R., & Galvão, L. S. (2012,
 1260 Nov). Effects of fire on above-ground forest biomass in the northern Brazilian

- 1261 Amazon. *J. Trop. Ecol.*, 28(6), 591–601. doi: 10.1017/S0266467412000636
- 1262 Marvin, D. C., Asner, G. P., Knapp, D. E., Anderson, C. B., Martin, R. E., Sinca,
1263 F., & Tupayachi, R. (2014, Dec). Amazonian landscapes and the bias in
1264 field studies of forest structure and biomass. *Proc. Natl. Acad. Sci. U. S. A.*,
1265 111(48), E5224–E5232. doi: 10.1073/pnas.1412999111
- 1266 Mascaro, J., Litton, C. M., Hughes, R. F., Uowolo, A., & Schnitzer, S. A. (2011,
1267 Nov). Minimizing bias in biomass allometry: Model selection and log-
1268 transformation of data. *Biotropica*, 43(6), 649–653. doi: 10.1111/
1269 j.1744-7429.2011.00798.x
- 1270 Matsunaga, T., Iwasaki, A., Tsuchida, S., Iwao, K., Tanii, J., Kashimura, O., . . .
1271 Tachikawa, T. (2017, Jul). Current status of hyperspectral imager suite
1272 (HISUI) onboard international space station (ISS). In *2017 IEEE interna-*
1273 *tional geoscience and remote sensing symposium (IGARSS)* (pp. 443–446). doi:
1274 10.1109/IGARSS.2017.8126989
- 1275 Mauya, E., Hansen, E., Gobakken, T., Bollandas, O., Malimbwi, R., & Næs-
1276 set, E. (2015, May). Effects of field plot size on prediction accuracy of
1277 aboveground biomass in airborne laser scanning-assisted inventories in trop-
1278 ical rain forests of Tanzania. *Carbon Balance Manage.*, 10(1), 10. doi:
1279 10.1186/s13021-015-0021-x
- 1280 Medvigy, D. M., Wofsy, S. C., Munger, J. W., Hollinger, D. Y., & Moorcroft, P. R.
1281 (2009, Jan). Mechanistic scaling of ecosystem function and dynamics in
1282 space and time: Ecosystem demography model version 2. *J. Geophys. Res.-*
1283 *Biogeosci.*, 114(G1), G01002. doi: 10.1029/2008JG000812
- 1284 Meister, K., Ashton, M. S., Craven, D., & Griscom, H. (2012). Carbon dynamics
1285 of tropical forests. In M. S. Ashton, M. L. Tyrrell, D. Spalding, & B. Gentry
1286 (Eds.), (pp. 51–75). Dordrecht, Netherlands: Springer Netherlands. doi: 10
1287 .1007/978-94-007-2232-3_4
- 1288 Mesquita, R. d. C. G., Massoca, P. E. d. S., Jakovac, C. C., Bentos, T. V., &
1289 Williamson, G. B. (2015, Aug). Amazon rain forest succession: Stochasticity
1290 or land-use legacy? *BioScience*, 65(9), 849–861. doi: 10.1093/biosci/biv108
- 1291 Meyer, V., Saatchi, S., Ferraz, A., Xu, L., Duque, A., García, M., & Chave, J. (2019,
1292 Mar). Forest degradation and biomass loss along the Chocó region of Colom-
1293 bia. *Carbon Balance Manage.*, 14(1), 2. doi: 10.1186/s13021-019-0117-9

- 1294 Meyer, V., Saatchi, S. S., Chave, J., Dalling, J. W., Bohlman, S., Fricker, G. A., ...
1295 Hubbell, S. (2013, Aug). Detecting tropical forest biomass dynamics from
1296 repeated airborne lidar measurements. *Biogeosciences*, *10*(8), 5421–5438. doi:
1297 10.5194/bg-10-5421-2013
- 1298 Miller, A. J. (1984, Nov). Selection of subsets of regression variables. *J. R. Stat. Soc.*
1299 *A-Gen.*, *147*(3), 389–425. doi: 10.2307/2981576
- 1300 Miller, S. D., Goulden, M. L., Hutyyra, L. R., Keller, M., Saleska, S. R., Wofsy, S. C.,
1301 ... de Camargo, P. B. (2011, Nov). Reduced impact logging minimally alters
1302 tropical rainforest carbon and energy exchange. *Proc. Natl. Acad. Sci. U. S.*
1303 *A.*, *108*(48), 19431–19435. doi: 10.1073/pnas.1105068108
- 1304 Moorcroft, P. R., Hurtt, G. C., & Pacala, S. W. (2001, Nov). A method for scaling
1305 vegetation dynamics: The Ecosystem Demography model (ED). *Ecol. Monogr.*,
1306 *71*(4), 557–586. doi: 10.1890/0012-9615(2001)071{0557:AMFSVD}{0557}2.0
1307 .CO;2
- 1308 Morton, D. C. (2016, Apr). Forest carbon fluxes: A satellite perspective. *Nature*
1309 *Clim. Change*, *6*(4), 346–348. doi: 10.1038/nclimate2978
- 1310 Morton, D. C., Le Page, Y., DeFries, R. S., Collatz, G. J., & Hurtt, G. C. (2013,
1311 Jun). Understorey fire frequency and the fate of burned forests in southern
1312 Amazonia. *Philos. Trans. R. Soc. B-Biol. Sci.*, *368*(1619), 20120163. doi:
1313 10.1098/rstb.2012.0163
- 1314 Ni-Meister, W., Jupp, D., & Dubayah, R. (2001, Sep). Modeling lidar waveforms
1315 in heterogeneous and discrete canopies. *IEEE T. Geosci. Remote Sens.*, *39*(9),
1316 1943–1958. doi: 10.1109/36.951085
- 1317 Norby, R. J., Gu, L., Haworth, I. C., Jensen, A. M., Turner, B. L., Walker, A. P.,
1318 ... Winter, K. (2017, Sep). Informing models through empirical relationships
1319 between foliar phosphorus, nitrogen and photosynthesis across diverse woody
1320 species in tropical forests of Panama. *New Phytol.*, *215*(4), 1425–1437. doi:
1321 10.1111/nph.14319
- 1322 Oleson, K. W., Lawrence, D. M., Bonan, G. B., Drewniak, B., Huang, M., Koven,
1323 C. D., ... Yang, Z.-L. (2013). *Technical description of version 4.5 of the*
1324 *community land model (CLM)* (Technical Report Nos. NCAR/TN-503+STR).
1325 Boulder, CO: NCAR. (420pp.) doi: 10.5065/D6RR1W7M
- 1326 Olivas, P. C., Oberbauer, S. F., Clark, D. B., Clark, D. A., Ryan, M. G., O'Brien,

- 1327 J. J., & Ordoñez, H. (2013, Aug). Comparison of direct and indirect methods
1328 for assessing leaf area index across a tropical rain forest landscape. *Agric. For.*
1329 *Meteorol.*, *177*, 110–116. doi: 10.1016/j.agrformet.2013.04.010
- 1330 Olson, D. M., Dinerstein, E., Wikramanayake, E. D., Burgess, N. D., Powell,
1331 G. V. N., Underwood, E. C., ... Kassem, K. R. (2001, Nov). Terrestrial
1332 ecoregions of the world: A new map of life on Earth. *BioScience*, *51*(11),
1333 933–938. doi: 10.1641/0006-3568(2001)051[0933:TEOTWA]2.0.CO;2
- 1334 Paracou Portal. (2016, Dec). *Paracou research station, a large-scale forest distur-*
1335 *bance experiment in Amazonia*. Retrieved 31 Jan 2020, from [https://paracou](https://paracou.cirad.fr)
1336 [.cirad.fr](https://paracou.cirad.fr)
- 1337 Pearson, T. R. H., Brown, S., Murray, L., & Sidman, G. (2017, Feb). Greenhouse
1338 gas emissions from tropical forest degradation: an underestimated source. *Car-*
1339 *bon Balance Manage.*, *12*(1), 3. doi: 10.1186/s13021-017-0072-2
- 1340 Pellegrini, A. F. A., Franco, A. C., & Hoffmann, W. A. (2016, Mar). Shifts in
1341 functional traits elevate risk of fire-driven tree dieback in tropical savanna and
1342 forest biomes. *Glob. Change Biol.*, *22*(3), 1235–1243. doi: 10.1111/gcb.13110
- 1343 Phillips, O. L., van der Heijden, G., Lewis, S. L., López-González, G., Aragão,
1344 L. E. O. C., Lloyd, J., ... Vilanova, E. (2010, Aug). Drought-mortality
1345 relationships for tropical forests. *New Phytol.*, *187*(3), 631-646. doi:
1346 10.1111/j.1469-8137.2010.03359.x
- 1347 Pinagé, E. R., Keller, M., Duffy, P., Longo, M., dos Santos, M. N., & Morton, D. C.
1348 (2019, Mar). Long-term impacts of selective logging on Amazon forest dy-
1349 namics from multi-temporal airborne LiDAR. *Remote Sens.*, *11*(6), 709. doi:
1350 10.3390/rs11060709
- 1351 Pinto, A., Amaral, P., Souza Jr., C. M., Veríssimo, A., Salomão, R., Gomes,
1352 G., & Balieiro, C. (2009). *Diagnóstico socioeconômico e florestal*
1353 *do município de Paragominas* (Technical Report). Belém,
1354 PA, Brazil: Instituto do Homem e Meio Ambiente da Amazônia
1355 (Imazon). (Available at [http://amazon.org.br/publicacoes/](http://amazon.org.br/publicacoes/diagnostico-socioeconomico-e-florestal-do-municipio-de-paragominas/)
1356 [diagnostico-socioeconomico-e-florestal-do-municipio-de-paragominas/](http://amazon.org.br/publicacoes/diagnostico-socioeconomico-e-florestal-do-municipio-de-paragominas/)
1357)
- 1358 Popescu, S. C., Zhao, K., Neuenschwander, A., & Lin, C. (2011, Nov). Satellite lidar
1359 vs. small footprint airborne lidar: Comparing the accuracy of aboveground

- 1360 biomass estimates and forest structure metrics at footprint level. *Remote Sens.*
1361 *Environ.*, *115*(11), 2786–2797. doi: 10.1016/j.rse.2011.01.026
- 1362 Potapov, P., Hansen, M. C., Laestadius, L., Turubanova, S., Yaroshenko, A., Thies,
1363 C., . . . Esipova, E. (2017, Jan). The last frontiers of wilderness: Tracking loss
1364 of intact forest landscapes from 2000 to 2013. *Sci. Adv.*, *3*(1), e1600821. doi:
1365 10.1126/sciadv.1600821
- 1366 Powell, T. L., Galbraith, D. R., Christoffersen, B. O., Harper, A., Imbuzeiro,
1367 H. M. A., Rowland, L., . . . Moorcroft, P. R. (2013, Oct). Confronting model
1368 predictions of carbon fluxes with measurements of Amazon forests subjected to
1369 experimental drought. *New Phytol.*, *200*(2), 350–365. doi: 10.1111/nph.12390
- 1370 Powers, J. S., & Tiffin, P. (2010, Aug). Plant functional type classifications in trop-
1371 ical dry forests in Costa Rica: leaf habit versus taxonomic approaches. *Funct.*
1372 *Ecol.*, *24*(4), 927–936. doi: 10.1111/j.1365-2435.2010.01701.x
- 1373 Priestley, C. H. B., & Taylor, R. J. (1972, Feb). On the assessment of surface heat
1374 flux and evaporation using large-scale parameters. *Mon. Wea. Rev.*, *100*(2),
1375 81–92. doi: 10.1175/1520-0493(1972)100<0081:OTAOSH>2.3.CO;2
- 1376 PRODES-INPE. (2018, Nov). *Taxas anuais de desmatamento*. Retrieved 9 Jan 2019,
1377 from <http://www.obt.inpe.br/prodes/index.php> (In Portuguese)
- 1378 Purves, D., & Pacala, S. (2008, Jun). Predictive models of forest dynamics. *Science*,
1379 *320*(5882), 1452–1453. doi: 10.1126/science.1155359
- 1380 Purves, D. W., Lichstein, J. W., Strigul, N., & Pacala, S. W. (2008, Nov).
1381 Predicting and understanding forest dynamics using a simple tractable
1382 model. *Proc. Natl. Acad. Sci. U. S. A.*, *105*(44), 17018–17022. doi:
1383 10.1073/pnas.0807754105
- 1384 Pütz, S., Groeneveld, J., Henle, K., Knogge, C., Martensen, A. C., Metz, M., . . .
1385 Huth, A. (2014, Oct). Long-term carbon loss in fragmented Neotropical
1386 forests. *Nat. Commun.*, *5*. doi: 10.1038/ncomms6037
- 1387 Pyle, E. H., Santoni, G. W., Nascimento, H. E. M., Hutyrá, L. R., Vieira, S., Cur-
1388 ran, D. J., . . . Wofsy, S. C. (2008, Mar). Dynamics of carbon, biomass, and
1389 structure in two Amazonian forests. *J. Geophys. Res.-Biogeosci.*, *113*(G1),
1390 G00B08. doi: 10.1029/2007JG000592
- 1391 Quesada, C. A., Miranda, A. C., Hodnett, M. G., Santos, A. J. B., Miranda, H. S.,
1392 & Breyer, L. M. (2004, Aug). Seasonal and depth variation of soil moisture in

- 1393 a burned open savanna (campo sujo) in central Brazil. *Ecol. Appl.*, *14*(sp4),
 1394 33–41. doi: 10.1890/01-6017
- 1395 Quesada, C. A., Phillips, O. L., Schwarz, M., Czimczik, C. I., Baker, T. R., Patiño,
 1396 S., . . . Lloyd, J. (2012, Sep). Basin-wide variations in Amazon forest structure
 1397 and function are mediated by both soils and climate. *Biogeosciences*, *9*(6),
 1398 2203–2246. doi: 10.5194/bg-9-2203-2012
- 1399 R Core Team. (2019). R: A language and environment for statistical computing
 1400 [Computer software manual]. Vienna, Austria. Retrieved from [http://www.R](http://www.R-project.org/)
 1401 [-project.org/](http://www.R-project.org/)
- 1402 Rappaport, D., Morton, D., Longo, M., Keller, M., Dubayah, R., & dos-Santos,
 1403 M. N. (2018, Jun). Quantifying long-term changes in carbon stocks and forest
 1404 structure from Amazon forest degradation. *Environ. Res. Lett.*, *13*(6), 065013.
 1405 doi: 10.1088/1748-9326/aac331
- 1406 Ray, D., Nepstad, D., & Moutinho, P. (2005, Oct). Micrometeorological and canopy
 1407 controls of fire susceptibility in a forested Amazon landscape. *Ecol. Appl.*,
 1408 *15*(5), 1664–1678. doi: 10.1890/05-0404
- 1409 Rödiger, E., Cuntz, M., Rammig, A., Fischer, R., Taubert, F., & Huth, A. (2018,
 1410 Apr). The importance of forest structure for carbon fluxes of the Amazon rain-
 1411 forest. *Environ. Res. Lett.*, *13*(5), 054013. doi: 10.1088/1748-9326/aabc61
- 1412 Russo, S., & Kitajima, K. (2016, Mar). The ecophysiology of leaf lifespan in
 1413 tropical forests: Adaptive and plastic responses to environmental hetero-
 1414 geneity. In G. Goldstein & L. S. Santiago (Eds.), *Tropical tree physiolo-*
 1415 *gy: Adaptations and responses in a changing environment* (Vol. 6, pp.
 1416 357–383). Cham, Switzerland: Springer International Publishing. doi:
 1417 10.1007/978-3-319-27422-5_17
- 1418 Sabine, C. L., Heimann, M., Artaxo, P., Bakker, D. C. E., Chen, C.-T. A., Field,
 1419 C. B., . . . Valentini, R. (2004). Current status and past trends of the global
 1420 carbon cycle. In C. B. Field & M. R. Raupach (Eds.), *The global carbon cy-*
 1421 *cle: integrating humans, climate, and the natural world* (Vol. 62, pp. 17–44).
 1422 Washington, DC, USA: Island Press.
- 1423 Santiago, L. S., & Wright, S. J. (2007, Feb). Leaf functional traits of tropical forest
 1424 plants in relation to growth form. *Funct. Ecol.*, *21*(1), 19–27. doi: 10.1111/j
 1425 .1365-2435.2006.01218.x

- 1426 Schimel, D., Schneider, F., & JPL Carbon and Ecosystem Participants. (2019). Flux
1427 towers in the sky: global ecology from space. *New Phytol.* (advance online
1428 publication) doi: 10.1111/nph.15934
- 1429 Schneider, F. D., Kükenbrink, D., Schaepman, M. E., Schimel, D. S., & Morsdorf,
1430 F. (2019, Apr). Quantifying 3D structure and occlusion in dense tropical
1431 and temperate forests using close-range LiDAR. *Agric. For. Meteorol.*, *268*,
1432 249–257. doi: 10.1016/j.agrformet.2019.01.033
- 1433 Schneider, F. D., Morsdorf, F., Schmid, B., Petchey, O. L., Hueni, A., Schimel,
1434 D. S., & Schaepman, M. E. (2017, Nov). Mapping functional diversity from
1435 remotely sensed morphological and physiological forest traits. *Nat. Commun.*,
1436 *8*(1), 1441. doi: 10.1038/s41467-017-01530-3
- 1437 Schwarz, G. (1978, Mar). Estimating the dimension of a model. *Ann. Stat.*, *6*(2),
1438 461–464. doi: 10.1214/aos/1176344136
- 1439 Sena, E. T., Silva Dias, M. A. F., Carvalho, L. M. V., & Silva Dias, P. L. (2018,
1440 Dec). Reduced wet-season length detected by satellite retrievals of cloudiness
1441 over Brazilian Amazonia: A new methodology. *J. Climate*, *31*(24), 9941–9964.
1442 doi: 10.1175/JCLI-D-17-0702.1
- 1443 Senior, R. A., Hill, J. K., Benedick, S., & Edwards, D. P. (2018, Mar). Tropical
1444 forests are thermally buffered despite intensive selective logging. *Glob. Change*
1445 *Biol.*, *24*(3), 1267–1278. doi: 10.1111/gcb.13914
- 1446 Shao, G., Stark, S. C., de Almeida, D. R., & Smith, M. N. (2019, Feb). Towards
1447 high throughput assessment of canopy dynamics: The estimation of leaf area
1448 structure in Amazonian forests with multitemporal multi-sensor airborne lidar.
1449 *Remote Sens. Environ.*, *221*(221), 1–13. doi: 10.1016/j.rse.2018.10.035
- 1450 Silva, C. V. J., Aragão, L. E. O. C., Barlow, J., Espírito-Santo, F., Young, P. J.,
1451 Anderson, L. O., . . . Xaud, H. A. M. (2018, Nov). Drought-induced Ama-
1452 zonian wildfires instigate a decadal-scale disruption of forest carbon dy-
1453 namics. *Philos. Trans. R. Soc. B-Biol. Sci.*, *373*(1760), 20180043. doi:
1454 10.1098/rstb.2018.0043
- 1455 Silvério, D. V., Brando, P. M., Bustamante, M. M., Putz, F. E., Marra, D. M.,
1456 Levick, S. R., & Trumbore, S. E. (2019, Mar). Fire, fragmentation, and wind-
1457 storms: a recipe for tropical forest degradation. *J. Ecol.*, *107*(2), 656–667. doi:
1458 10.1111/1365-2745.13076

- 1459 Souza Jr., C. M., Siqueira, J., Sales, M. H., Fonseca, A., Ribeiro, J., Numat, ...
 1460 Barlow, J. B. (2013, Oct). Ten-year Landsat classification of deforestation and
 1461 forest degradation in the Brazilian Amazon. *Remote Sens.*, 5(11), 5493–5513.
 1462 doi: 10.3390/rs5115493
- 1463 Spracklen, D., Baker, J., Garcia-Carreras, L., & Marsham, J. (2018, Oct). The ef-
 1464 fects of tropical vegetation on rainfall. *Ann. Rev. Environ. Res.*, 43(1), 193–
 1465 218. doi: 10.1146/annurev-environ-102017-030136
- 1466 Stahl, C., Hérault, B., Rossi, V., Burban, B., Bréchet, C., & Bonal, D. (2013,
 1467 Dec). Depth of soil water uptake by tropical rainforest trees during dry
 1468 periods: does tree dimension matter? *Oecologia*, 173(4), 1191–1201. doi:
 1469 10.1007/s00442-013-2724-6
- 1470 Stark, S. C., Leitold, V., Wu, J. L., Hunter, M. O., de Castilho, C. V., Costa,
 1471 F. R. C., ... Saleska, S. R. (2012, Dec). Amazon forest carbon dynamics
 1472 predicted by profiles of canopy leaf area and light environment. *Ecol. Lett.*,
 1473 15(12), 1406–1414. doi: 10.1111/j.1461-0248.2012.01864.x
- 1474 Stavros, E. N., Schimel, D., Pavlick, R., Serbin, S., Swann, A., Duncanson, L., ...
 1475 Wennberg, P. (2017, Jun). ISS observations offer insights into plant function.
 1476 *Nature Ecol. Evol.*, 1, 0194. doi: 10.1038/s41559-017-0194
- 1477 Stovall, A. E., Anderson Teixeira, K. J., & Shugart, H. H. (2018, Nov). Assessing
 1478 terrestrial laser scanning for developing non-destructive biomass allometry.
 1479 *Forest Ecol. Manag.*, 427, 217–229. doi: 10.1016/j.foreco.2018.06.004
- 1480 Strigul, N., Pristinski, D., Purves, D., Dushoff, J., & Pacala, S. (2008, Nov). Scal-
 1481 ing from trees to forests: tractable macroscopic equations for forest dynamics.
 1482 *Ecol. Monogr.*, 78(4), 523–545. doi: 10.1890/08-0082.1
- 1483 Sullivan, M. J. P., Lewis, S. L., Affum-Baffoe, K., Castilho, C., Costa, F., Sanchez,
 1484 A. C., ... Phillips, O. L. (2020, May). Long-term thermal sensitivity of earth’s
 1485 tropical forests. *Science*, 368(6493), 869–874. doi: 10.1126/science.aaw7578
- 1486 Sustainable Landscapes Brazil. (2019, Nov). Retrieved 9 Jan 2019, from [https://](https://www.paisagenslidar.cnptia.embrapa.br/webgis/)
 1487 www.paisagenslidar.cnptia.embrapa.br/webgis/
- 1488 Swann, A. L. S., & Koven, C. D. (2017, Aug). A direct estimate of the seasonal
 1489 cycle of evapotranspiration over the Amazon Basin. *J. Hydrometeor.*, 18(8),
 1490 2173–2185. doi: 10.1175/JHM-D-17-0004.1
- 1491 Swann, A. L. S., Longo, M., Knox, R. G., Lee, E., & Moorcroft, P. R. (2015,

- 1492 Dec). Future deforestation in the Amazon and consequences for South
 1493 American climate. *Agric. For. Meteorol.*, *214–215*, 12–24. doi: 10.1016/
 1494 j.agrformet.2015.07.006
- 1495 Tang, H., & Dubayah, R. (2017, Mar). Light-driven growth in Amazon evergreen
 1496 forests explained by seasonal variations of vertical canopy structure. *Proc.*
 1497 *Natl. Acad. Sci. U. S. A.*, *114*(10), 2640–2644. doi: 10.1073/pnas.1616943114
- 1498 Thonicke, K., Spessa, A., Prentice, I. C., Harrison, S. P., Dong, L., & Carmona-
 1499 Moreno, C. (2010, Jun). The influence of vegetation, fire spread and fire
 1500 behaviour on biomass burning and trace gas emissions: results from a process-
 1501 based model. *Biogeosciences*, *7*(6), 1991–2011. doi: 10.5194/bg-7-1991-2010
- 1502 Tyukavina, A., Hansen, M. C., Potapov, P. V., Krylov, A. M., & Goetz, S. J. (2016,
 1503 Feb). Pan-tropical hinterland forests: mapping minimally disturbed forests.
 1504 *Global Ecol. Biogeogr.*, *25*(2), 151–163. doi: 10.1111/geb.12394
- 1505 Tyukavina, A., Hansen, M. C., Potapov, P. V., Stehman, S. V., Smith-Rodriguez,
 1506 K., Okpa, C., & Aguilar, R. (2017, Apr). Types and rates of forest distur-
 1507 bance in Brazilian Legal Amazon, 2000–2013. *Sci. Adv.*, *3*(4), e1601047. doi:
 1508 10.1126/sciadv.1601047
- 1509 Uhl, C., & Buschbacher, R. (1985, Dec). A disturbing synergism between cattle
 1510 ranch burning practices and selective tree harvesting in the eastern Amazon.
 1511 *Biotropica*, *17*(4), 265–268. doi: 10.2307/2388588
- 1512 Uhl, C., & Kauffman, J. B. (1990, Apr). Deforestation, fire susceptibility, and poten-
 1513 tial tree responses to fire in the Eastern Amazon. *Ecology*, *71*(2), 437–449. doi:
 1514 10.2307/1940299
- 1515 van der Ent, R. J., Savenije, H. H. G., Schaeffli, B., & Steele-Dunne, S. C. (2010,
 1516 Sep). Origin and fate of atmospheric moisture over continents. *Water Resour.*
 1517 *Res.*, *46*(9), W09525. doi: 10.1029/2010WR009127
- 1518 VanWey, L. K., D’Antona, A. O., & Brondízio, E. S. (2007, Jan). Household de-
 1519 mographic change and land use/land cover change in the Brazilian Amazon.
 1520 *Popul. Environ.*, *28*(3), 163–185. doi: 10.1007/s11111-007-0040-y
- 1521 Veríssimo, A., Barreto, P., Mattos, M., Tarifa, R., & Uhl, C. (1992, Dec). Logging
 1522 impacts and prospects for sustainable forest management in an old Amazonian
 1523 frontier: The case of Paragominas. *Forest Ecol. Manag.*, *55*(1–4), 169–199. doi:
 1524 10.1016/0378-1127(92)90099-U

- 1525 Vincent, G., Antin, C., Laurans, M., Heurtebize, J., Durrieu, S., Lavalley, C., &
 1526 Dauzat, J. (2017, Sep). Mapping plant area index of tropical evergreen for-
 1527 est by airborne laser scanning. a cross-validation study using LAI2200 optical
 1528 sensor. *Remote Sens. Environ.*, *198*, 254–266. doi: 10.1016/j.rse.2017.05.034
- 1529 von Caemmerer, S. (2000). *Biochemical models of leaf photosynthesis* (No. 2).
 1530 Collingwood, VIC, Australia: CSIRO Publishing. doi: 10.1006/anbo.2000
 1531 .1296
- 1532 von Randow, C., Manzi, A. O., Kruijt, B., de Oliveira, P. J., Zanchi, F. B., Silva,
 1533 R. L., . . . Kabat, P. (2004, Jun). Comparative measurements and sea-
 1534 sonal variations in energy and carbon exchange over forest and pasture
 1535 in south west amazonia. *Theor. Appl. Climatol.*, *78*(1–3), 5–26. doi:
 1536 10.1007/s00704-004-0041-z
- 1537 Wagner, F., Rossi, V., Stahl, C., Bonal, D., & Hérault, B. (2013, Nov). Asyn-
 1538 chronism in leaf and wood production in tropical forests: a study combining
 1539 satellite and ground-based measurements. *Biogeosciences*, *10*(11), 7307–7321.
 1540 doi: 10.5194/bgd-10-8247-2013
- 1541 Walker, W. S., Gorelik, S. R., Baccini, A., Aragon-Osejo, J. L., Josse, C., Meyer,
 1542 C., . . . Schwartzman, S. (2020). The role of forest conversion, degradation,
 1543 and disturbance in the carbon dynamics of Amazon indigenous territories and
 1544 protected areas. *Proc. Natl. Acad. Sci. U. S. A.*. (advance online publication)
 1545 doi: 10.1073/pnas.1913321117
- 1546 Wright, I. J., Reich, P. B., Westoby, M., Ackerly, D. D., Baruch, Z., Bongers, F.,
 1547 . . . Villar, R. (2004, Apr). The worldwide leaf economics spectrum. *Nature*,
 1548 *428*(6985), 821–827. doi: 10.1038/nature02403
- 1549 Wright, J. S., Fu, R., Worden, J. R., Chakraborty, S., Clinton, N. E., Risi, C., . . .
 1550 Yin, L. (2017, Aug). Rainforest-initiated wet season onset over the south-
 1551 ern Amazon. *Proc. Natl. Acad. Sci. U. S. A.*, *114*(32), 8481–8486. doi:
 1552 10.1073/pnas.1621516114
- 1553 Wu, M., Schurgers, G., Ahlström, A., Rummukainen, M., Miller, P. A., Smith, B.,
 1554 & May, W. (2017, May). Impacts of land use on climate and ecosystem pro-
 1555 ductivity over the Amazon and the South American continent. *Environ. Res.*
 1556 *Lett.*, *12*(5), 054016. doi: 10.1088/1748-9326/aa6fd6
- 1557 Yang, Y., Donohue, R. J., & McVicar, T. R. (2016, Oct). Global estimation of ef-

- 1558 fective plant rooting depth: Implications for hydrological modeling. *Water Re-*
1559 *sour. Res.*, *52*(10), 8260–8276. doi: 10.1002/2016WR019392
- 1560 Zemp, D. C., Schleussner, C.-F., Barbosa, H. M. J., Hirota, M., Montade, V., Sam-
1561 paio, G., . . . Rammig, A. (2017, Mar). Self-amplified Amazon forest loss
1562 due to vegetation-atmosphere feedbacks. *Nat. Commun.*, *8*, 14681. doi:
1563 10.1038/ncomms14681
- 1564 Zhang, K., Castanho, A. D. d. A., Galbraith, D. R., Moghim, S., Levine, N., Bras,
1565 R. L., . . . Moorcroft, P. R. (2015, Jul). The fate of Amazonian ecosystems
1566 over the coming century arising from changes in climate, atmospheric CO₂ and
1567 land-use. *Glob. Change Biol.*, *21*(7), 2569–2587. doi: 10.1111/gcb.12903